

General relativistic effects on pulsar radiation

Dong-Hoon Kim^{1,2,*} and Sascha Trippe^{2,†}

¹*The Research Institute of Basic Sciences, Seoul National University, Seoul 08826, Republic of Korea*

²*Department of Physics and Astronomy, Seoul National University, Seoul 08826, Republic of Korea*

ABSTRACT

The magnetosphere of, and electromagnetic (EM) radiation from pulsars are usually described in the framework of classical electrodynamics. For some pulsars, however, whose emission heights are relatively close to the surface of the neutron star, general relativistic effects might modify the emission from the pulsar. We consider a magnetic dipole model of a pulsar to investigate general relativistic effects on EM radiation from it. Our study includes general relativistic modifications applicable to some significant issues in pulsar astronomy, such as the magnetosphere structure and pulse profiles. We implement computation of the magnetic field in the pulsar magnetosphere from a solution to Maxwell’s equations defined in the strongly curved spacetime around a pulsar and find that the field exhibits a strong gravitational effect. The effect modifies curvature radiation of a pulsar, which then leads to modifications of the pulse profiles of radio emission. We take the pulsar PSR J1828–1101 as an example and work out Stokes parameters to simulate the pulse profiles for its main and interpulse emissions theoretically, which exhibit the gravitational effects clearly; however, their testability is beyond the current detection capabilities, with the absolute magnitude of the pulse profiles not being precisely predictable.

I. INTRODUCTION

Despite decades of study, pulsars still pose challenges for both observations and theory. To first order, pulsars are described as “cosmic light houses”: neutron stars with strong magnetic dipole fields rotating about an axis which is misaligned with respect to the magnetic axis. Electrically charged particles are accelerated along the magnetic field lines, especially around the magnetic poles, and emit electromagnetic (EM) radiation across the entire EM spectrum from radio to γ -rays. If the rotation axis of the neutron star and the magnetic axis are tilted relative to each other, a distant observer may observe characteristic radiation pulses. Electrodynamics dictates that the loss of energy due to radiation leads to a characteristic slowdown rate \dot{P} of the pulsar period P , in good agreement with observations [1]. However, the complex physical processes involved in shaping pulsar magnetospheres and radiation mechanisms – particle acceleration, non-thermal emission, pair creation, relativistic reconnection, and (special) relativistic magneto-hydrodynamics – require exhaustive theoretical and numerical studies to achieve a more complete understanding of pulsar physics [2]. Understanding the emission from, and brightness of, pulsars across the EM spectrum has consequences beyond neutron star physics. One example

for this is the observation of γ radiation from the Galactic centre for which the annihilation of exotic dark matter particles was suggested as source. Depending on the spectral distribution of pulsar emission, radiation from a large population of millisecond pulsars explains the signal equally well, thus eliminating the need for exotic explanations [3, 4].

One aspect that is usually neglected is the impact of general relativity on the radio emission. Depending on where the emission takes place, gravity can have a noticeable effect on the pulse profiles and the luminosity of a pulsar from a theoretical perspective; therefore, its effect should be taken into consideration for precise and accurate analyses of observational data. Neutron stars have masses between 1.2 and 2.0 solar masses and radii of about 11 km [5], corresponding to about two to three Schwarzschild radii. This means that general relativistic effects are important at least close to their surfaces. The radiation received by a distant observer is emitted at a specific “emission height” from the centre of the neutron star: the peak frequency of curvature radiation, assumed to be the observing frequency, is a function of particle Lorentz factor and curvature radius; for a given frequency and Lorentz factor, the curvature radius and thus the emission height follow [6]. For “classical” pulsars with rotation periods on the order of one second, the bulk of the EM radiation is emitted at emission heights several hundred kilometers above the surface, corresponding to roughly one hundred Schwarzschild radii [7]; this greatly

* ki13130@gmail.com

† trippe@snu.ac.kr; corresponding author

reduces relativistic effects and usually justifies neglecting them. Even though, substantial relativistic effects may be expected at least for some pulsars. A natural upper limit for the emission height is provided by the light cylinder radius [2] which is 48 km, about 10 Schwarzschild radii, for a pulsar with a period of one millisecond. This suggests that millisecond pulsars are candidates for the detection of relativistic effects in their radiation.¹ Emission heights vary substantially between objects; radio observations have found emission heights below 100 km for several pulsars [9, 10], with the smallest value being about 25 km for the millisecond pulsar J1022+1001 [9].

Previous studies of general relativistic effects were mostly focused on the EM field geometry around a rotating neutron star. Sengupta [11] investigated the importance of general relativistic corrections to the induced electric field exterior to a neutron star by considering the simplest aligned vacuum and nonvacuum magnetosphere models. Konno and Kojima [12] worked out EM fields around a rotating star endowed with an aligned dipole magnetic field by solving Maxwell's equations in a slowly rotating Kerr spacetime. Rezzolla et al. [13] obtained analytic solutions of Maxwell's equations in the internal and external background spacetime of a slowly rotating misaligned magnetized neutron star. Ruiz et al. [14] used numerical simulations to estimate the general relativistic spin-down luminosity of pulsars. Pétri [15] performed time-dependent simulations of Maxwell's equations in a stationary background metric in the slow-rotation approximation and found that the Poynting flux observed at a large distance is substantially higher in the general relativistic case compared to the non-relativistic case.

In this work, we investigate general relativistic modifications of pulsar radiation analytically, by considering a magnetic dipole model which is an 'oblique' (or misaligned) rotator with an inclination angle. We derive expressions for a general relativistic description of the pulsar magnetosphere and the corresponding pulsar energetics and EM radiation. Largely, our analysis proceeds in two steps through Sections II and III. In Section II, general relativistic modifications of the magnetic field around a rotating neutron star are studied. To this end, we specially prescribe a rotating Schwarzschild ge-

ometry, which is modified from a slowly rotating Kerr spacetime but well suited to solving Maxwell's equations for the magnetic field exterior to an oblique rotator. The results obtained in Section II are fully employed to develop our analysis for EM radiation in Section III, such as very low-frequency magnetic dipole radiation for pulsar spin-down and curvature radiation from the pulsar PSR J1828–1101.

II. ELECTRODYNAMICS IN THE PULSAR MAGNETOSPHERE

A. Geometric Configuration of an Obliquely Rotating Pulsar

We consider a magnetic dipole model of a pulsar in a general configuration: a rotating neutron star having the magnetic field around it, which can be well-approximated to be that of a pure magnetic dipole [11, 16], with its magnetic axis tilted from its rotation axis by an angle α . The spacetime geometry around the pulsar is strongly curved due to the immense gravitation of the neutron star. An obliquely rotating pulsar can be modeled using the Kerr geometry [13]; more effectively, the geometry can be described by a Kerr metric in the slow rotation limit:

$$ds^2 = -f(r) c^2 dt^2 + \frac{1}{f(r)} dr^2 + r^2 d\theta^2 + r^2 \sin^2 \theta d\tilde{\phi}^2 + \mathcal{O}(a^2), \quad (1)$$

where $f(r) \equiv 1 - 2GM/(c^2 r)$, with G being the gravitational constant, c being the speed of light and M being the total mass of the neutron star, and

$$\tilde{\phi} \equiv \phi - \Omega_{\text{f.d.}} t, \quad (2)$$

where

$$\Omega_{\text{f.d.}} = 2GJ/(c^2 r^3) = 2GMa/(cr^3) \quad (3)$$

is the "frame-dragging" angular frequency of the pulsar with J being the angular momentum and $a = J/(Mc)$ being the Kerr parameter. Here $\mathcal{O}(a^2) \sim \mathcal{O}(\Omega_{\text{f.d.}}^2)$ represents any higher order terms than linear in $a \sim \Omega_{\text{f.d.}}$, which would come from the full Kerr metric when expanded with respect to a , can be cast off in the slow rotation limit.

Our pulsar model is graphically illustrated in Fig. 1. Note that the magnetic axis, which coincides with the magnetic dipole and the radiation beam direction, is inclined from the rotation axis by the angle α . Also,

¹ As of October 27, 2020, the number of pulsars listed in the ATFN Pulsar Catalogue [8] with $P \leq 5$ ms was 257, out of a total of 2871 pulsars.

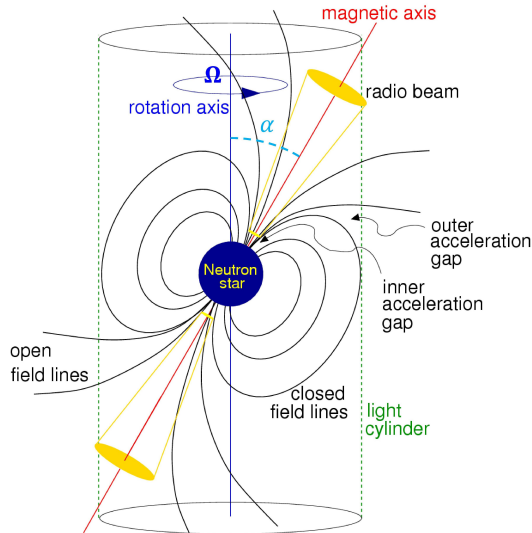


FIG. 1: A graphical illustration of our pulsar model: the magnetic axis is inclined from the rotation axis by the angle α . (Credit: Lorimer and Kramer [18], reproduced with some modifications.)

for the rest of our analysis, it should be noted that $\Omega = |\mathbf{\Omega}| = 2\pi/P$ denotes the pulsar rotation frequency, which should be distinguished from the frame-dragging frequency $\Omega_{f.d.}$ as defined by Eq. (3) above. While $\Omega_{f.d.}$ drops rapidly as one moves away from the pulsar surface, Ω is a *nearly fixed* value through the measurement of the rotation period P . One may express the angular momentum J as

$$J = k^2 MR_*^2 \Omega, \quad (4)$$

where $k^2 \simeq 0.4$ depending on the neutron star equation of state and R_* denotes the radius of the star [17]. Using this, we can relate the frame-dragging frequency $\Omega_{f.d.}$ to the rotation frequency Ω [17]:

$$\Omega_{f.d.} = \Omega_* (R_*/r)^3, \quad (5)$$

where

$$\Omega_* \equiv \Omega_{f.d.}(r = R_*) = [2k^2 GM / (c^2 R_*)] \Omega \quad (6)$$

is the frame-dragging frequency defined at the stellar surface given by means of Eqs. (3) and (4).²

² A neutron star has a hard surface while a black hole has an event horizon. With this distinction, a rotating neutron star is well-characterized by the frame-dragging angular frequency evaluated at its surface.

B. EM Fields of an Obliquely Rotating Pulsar

In Section II A we have described the configuration of our pulsar: the main features are (i) the star's magnetic axis is tilted from its rotation axis by the angle α , (ii) the star is slowly rotating at the frequency $\Omega = 2\pi/P$, where P is the rotation period obtained through measurement. Now, the spacetime geometry described by Eq. (1) is corotating slowly at the frame-dragging frequency $\Omega_{f.d.}$, which varies with the radial position r as given by Eq. (3), rather than the pulsar rotation frequency Ω . Analytical solutions of Maxwell's equations in this geometry are available in the literature; e.g., [13]. However, in the present analysis, we are concerned only with the magnetic field outside the neutron star, which corresponds to part of the stationary exterior vacuum solution of Maxwell's equations for a misaligned magnetized rotator as obtained by [13]. From the solution, it should be noted that general relativistic corrections due to the frame-dragging effect are not present in the expression for the magnetic field in the slow rotation limit; that is, the expression is given in terms of the pulsar rotation frequency Ω but not the frame-dragging frequency $\Omega_{f.d.}$. Then one might consider that the same result can be obtained by solving Maxwell's equations for the magnetic field in a frame that corotates with the pulsar at the frequency Ω and then performing the coordinate transformation between this frame and the inertial frame. This alternative method, albeit much simpler to implement, is fully legitimate as long as our attention is restricted to the magnetic field exterior to the slowly rotating star. Also, it is consistent with our analysis for curvature radiation developed in Section III B.³ The method is described in detail below.

1. Transformation between the Inertial Frame and the Corotating Frame

Following the argument regarding the magnetic field exterior to the slowly rotating star as given above, we can simplify our analysis by replacing $\Omega_{f.d.}$ with the pulsar rotation frequency $\Omega = 2\pi/P$, which is in correspon-

³ In order to describe curvature radiation, we introduce quantities such as the curvature radius of a charge's trajectory along a magnetic field line, the Stokes parameters defined from the Liénard–Wiechert EM field due to a charge moving along a magnetic field line, etc., which are derived in the corotating frame first and then transformed to the inertial frame.

dence with observation through the measurement of the rotation period P . As $\tilde{\phi}$ is modified from Eq. (2):

$$\tilde{\phi} = \phi - \Omega t, \quad (7)$$

where $\Omega_{f,d}$ has been replaced by Ω , the new geometry modified from Eq. (1) is spherically symmetric apart from $\mathcal{O}(a^2) \sim \mathcal{O}(R_*(v_*/c)^2)$, where $v_* \equiv \Omega R_*$ is the star's spinning velocity at its surface.

The spherical symmetry of the modified geometry is maintained under the transformation of coordinates from a frame $(t, r, \theta, \tilde{\phi})$ to another (t, r, θ', ϕ') on the 2-sphere. Suppose that (x, y, z) and (x', y', z') are the Cartesian frames converted from the spherical frames (r, θ, ϕ) and (r, θ', ϕ') , respectively: following the usual convention, $\theta[\theta']$ is defined as the polar angle measured from the $z[z']$ -axis while $\phi[\phi']$ is the azimuthal angle around the $z[z']$ -axis, with the z' -axis being tilted from the z -axis by the angle α . As illustrated in Fig. 1, we may set

$$\mathbf{M} = \begin{bmatrix} 1 & 0 & 0 \\ 0 & \frac{\cos \alpha \sin \theta - \sin \alpha \cos \theta \cos(\phi - \Omega t)}{\sin \theta'} & \frac{-\sin \alpha \sin(\phi - \Omega t)}{\sin \theta'} \\ 0 & \frac{\sin \alpha \sin(\phi - \Omega t)}{\sin \theta'} & \frac{\cos \alpha \sin \theta - \sin \alpha \cos \theta \cos(\phi - \Omega t)}{\sin \theta'} \end{bmatrix}, \quad (9)$$

with θ' being expressed via

$$\cos \theta' = \cos \alpha \cos \theta + \sin \alpha \sin \theta \cos(\phi - \Omega t). \quad (10)$$

This gives a definition of the ‘‘magnetic colatitude’’ [19]; that is, the corotating polar angle evaluated in the inertial frame.

Letting $(\mathbf{e}_{\hat{r}}, \mathbf{e}_{\hat{\theta}}, \mathbf{e}_{\hat{\phi}})$ and $(\mathbf{e}_{\hat{r}'}, \mathbf{e}_{\hat{\theta}'}, \mathbf{e}_{\hat{\phi}'})$ refer to the inertial frame and the corotating frame, respectively, Eq. (9) represents the transformation between these frames. Later in Section II B 3, this will be employed to determine the EM fields for our obliquely rotating pulsar as viewed by an observer in the inertial frame.

2. Solving Maxwell's Equations in the Corotating Frame

We may identify the magnetic axis of our pulsar with the z' -axis as described in Section II B 1. Now, taking advantage of the spherical symmetry, the new geometry modified from (1), with (2) being replaced by (7) can be reformed to another Schwarzschild metric apart from

the rotation axis and the magnetic axis of our pulsar to be along the z -axis and the z' -axis, respectively. Then it follows that the frame (x', y', z') is rotated relative to the frame (x, y, z) about the z -axis by the amount of rotation Ωt , while keeping the angle α between the z -axis and the z' -axis. Fig. 2 illustrates how these two frames are related to each other. The transformation between the frames (r, θ, ϕ) and (r, θ', ϕ') can be determined by way of the transformation between the frames (x, y, z) and (x', y', z') . This would require a somewhat involved analysis, and therefore we present only the result here and the technical details are provided in Appendix A. With the basis vectors $(\mathbf{e}_{\hat{r}}, \mathbf{e}_{\hat{\theta}}, \mathbf{e}_{\hat{\phi}})$ and $(\mathbf{e}_{\hat{r}'}, \mathbf{e}_{\hat{\theta}'}, \mathbf{e}_{\hat{\phi}'})$ for the frames (r, θ, ϕ) and (r, θ', ϕ') , respectively, it is shown that the two frames are related to each other:

$$\begin{bmatrix} \mathbf{e}_{\hat{r}} \\ \mathbf{e}_{\hat{\theta}} \\ \mathbf{e}_{\hat{\phi}} \end{bmatrix} = \mathbf{M} \begin{bmatrix} \mathbf{e}_{\hat{r}'} \\ \mathbf{e}_{\hat{\theta}'} \\ \mathbf{e}_{\hat{\phi}'} \end{bmatrix}, \quad (8)$$

where

$\mathcal{O}(a^2)$:

$$ds^2 = -f(r) c^2 dt^2 + \frac{1}{f(r)} dr^2 + r^2 d\theta'^2 + r^2 \sin^2 \theta' d\phi'^2 + \mathcal{O}(a^2), \quad (11)$$

where θ' is the polar angle measured from the z' -axis, i.e., magnetic axis and ϕ' is the azimuthal angle around this axis. For an observer sitting in the frame (t, r, θ', ϕ') , electromagnetism in our pulsar magnetosphere will be described by the Maxwell's equations in the geometry (11):

$$\nabla^2 A_a - R_a{}^b A_b = -\frac{4\pi}{c} j_a, \quad (12)$$

where ∇^2 denotes the curved spacetime d'Alembertian, A_a represents the EM vector potential, j_a is the current density, R_{ab} is the Ricci tensor, and the indices a, b, \dots refer to the coordinates (t, r, θ', ϕ') .

Following Petterson [16], we can express the current density in Eq. (12) as

$$j^{\phi'} = \left(1 - \frac{2m}{r}\right)^{1/2} \frac{\delta(r - R_o) \delta(\cos \theta') I}{r^2}, \quad (13)$$

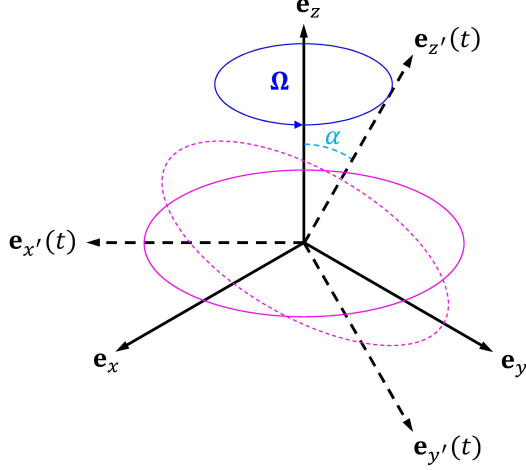


FIG. 2: The inertial frame $\mathbf{x} \equiv (x, y, z)$ and the obliquely corotating frame $\mathbf{x}' \equiv (x', y', z')$. The z' -axis of the latter rotates around the z -axis of the former at the angular frequency Ω , keeping the angle α between the two axes. The relation between the two frames is described mathematically by Eqs. (A1)-(A3) in Appendix A.

where $m \equiv GM/c^2$ and I is a static current loop of radius R_o , encircling the equator of the neutron star, i.e., $\theta' = \pi/2$.⁴ Then a solution to Eq. (12) is obtained as [16, 20, 21]

$$A_{\phi'} = -\frac{3\mu \sin^2 \theta'}{8m^3} \left[r^2 \ln \left(1 - \frac{2m}{r} \right) + 2mr \left(1 + \frac{m}{r} \right) \right], \quad (14)$$

where μ is the magnetic dipole moment associated with

the current density $j_{\phi'}$, and leads to [16]⁵

$$\mu = \pi R_o^2 \left(1 - \frac{2m}{R_o} \right)^{1/2} I. \quad (15)$$

In the same frame, using Eq. (14), we obtain the components of the magnetic field from the definition of the EM field-strength tensor, $F_{ab} \equiv A_{b,a} - A_{a,b}$, where the comma followed by the subscript indicates partial differentiation with respect to the subscript [11, 16]:

$$\begin{aligned} B_{\hat{r}} &= F_{\hat{\theta}'\hat{\phi}'} = F_{\theta'\phi'} \lambda_{\hat{\theta}'}^{\theta'} \lambda_{\hat{\phi}'}^{\phi'} \\ &= -\frac{3\mu \cos \theta'}{4m^3} \left[\ln \left(1 - \frac{2m}{r} \right) + \frac{2m}{r} \left(1 + \frac{m}{r} \right) \right], \quad (16) \\ B_{\hat{\theta}'} &= F_{\hat{r}\hat{\phi}'} = F_{r\phi'} \lambda_{\hat{r}}^r \lambda_{\hat{\phi}'}^{\phi'} \\ &= \frac{3\mu \sin \theta'}{4m^3} \left[\ln \left(1 - \frac{2m}{r} \right) + \frac{m}{r} \left(\left(1 - \frac{2m}{r} \right)^{-1} + 1 \right) \right] \\ &\quad \times \left(1 - \frac{2m}{r} \right)^{1/2}, \quad (17) \end{aligned}$$

where the indices with a ‘hat’ ($\hat{}$) denote the components in a local Lorentz frame and $\lambda_{\hat{b}}^a$ represents the orthonormal tetrad of the local Lorentz frame for the geometry (11), the non-vanishing components of which are given by

$$\begin{aligned} &\left\{ \lambda_{\hat{t}}^t, \lambda_{\hat{r}}^r, \lambda_{\hat{\theta}'}^{\theta'}, \lambda_{\hat{\phi}'}^{\phi'} \right\} \\ &= \left\{ \left(1 - \frac{2m}{r} \right)^{-1/2}, \left(1 - \frac{2m}{r} \right)^{1/2}, \frac{1}{r}, \frac{1}{r \sin \theta'} \right\}. \quad (18) \end{aligned}$$

Dropping the ‘prime’ signs from this, the orthonormal tetrad defined in the inertial frame (t, r, θ, ϕ) is also expressed in the same manner.

It should be noted that the magnetic field components given by Eqs. (16) and (17) above would be the values as observed in the corotating frame, and hence that they do

⁴ I is the total current through the $\hat{r}\hat{\theta}'$ -plane as defined in the local Lorentz frame:

$$I = \iint j^{\hat{\phi}'} \hat{r} \hat{\theta}' d\hat{\theta}',$$

where $j^{\hat{\phi}'} = j^{\phi'} \left(\lambda_{\hat{\phi}'}^{\phi'} \right)^{-1}$, $d\hat{r} = dr \left(\lambda_{\hat{r}}^r \right)^{-1}$ and $d\hat{\theta}' = d\theta \left(\lambda_{\hat{\theta}'}^{\theta'} \right)^{-1}$ by means of the tetrad (18) [16].

⁵ A general relativistic effect is taken into consideration in this expression: it depends on the mass of the star M through $m = GM/c^2$. For example, for a standard neutron star with $R_* \simeq 4GM/c^2$, we have $\mu \simeq \pi R_*^2 I / \sqrt{2}$ with $R_o = R_*$ substituted into the expression, which contrasts with $\mu = \pi R_*^2 I$, the value in the flat spacetime limit $m \rightarrow 0$. On the other hand, we find that μ vanishes in the limit $R_* \rightarrow 2GM/c^2$, i.e., approaching the event horizon. This corresponds to the vanishing of the magnetic field for an observer at infinity when the source approaches the horizon. This notion is in accordance with a theorem by Price [22]: during the process of gravitational collapse, all EM multipole moments of the collapsing matter, except the electric monopole moment, must disappear [16, 22].

not exhibit any effect of rotation of our star; as if the star were static, with its spacetime geometry being described by Eq. (11). Next, we will find how the star's rotation affects the EM fields observed in the inertial frame.

3. EM Fields as Observed in the Inertial Frame

For an observer in the inertial frame, electromagnetism of the pulsar should be different from that observed in the corotating frame as the rotation of the star affects our observation of the EM fields.

First, the vector potential (14) should be transformed from the corotating frame to the inertial frame:

$$\begin{aligned}
A_\theta &= A_{\phi'} \lambda_{\hat{\phi}'}^{\phi'} M_{\hat{\theta}}^{\hat{\phi}'} \left(\lambda_{\hat{\theta}}^\theta \right)^{-1} \\
&= \frac{3\mu \sin \alpha \sin(\phi - \Omega t)}{8m^3} \\
&\times \left[r^2 \ln \left(1 - \frac{2m}{r} \right) + 2mr \left(1 + \frac{m}{r} \right) \right], \quad (19) \\
A_\phi &= A_{\phi'} \lambda_{\hat{\phi}'}^{\phi'} M_{\hat{\phi}}^{\hat{\phi}'} \left(\lambda_{\hat{\phi}}^\phi \right)^{-1} \\
&= -\frac{3\mu \sin \theta [\cos \alpha \sin \theta - \sin \alpha \cos \theta \cos(\phi - \Omega t)]}{8m^3} \\
&\times \left[r^2 \ln \left(1 - \frac{2m}{r} \right) + 2mr \left(1 + \frac{m}{r} \right) \right], \quad (20)
\end{aligned}$$

where $M_{\hat{a}}^{\hat{b}}$ is to be read off from the transformation matrix given by Eq. (9), and $\lambda_{\hat{b}}^{\hat{a}}$ is given by Eq. (18).

The magnetic field in the inertial frame can be determined through $F_{ab} = A_{b,a} - A_{a,b}$, together with Eqs. (19)

and (20) and using Eq. (18):⁶

$$\begin{aligned}
B_{\hat{r}} &= F_{\hat{\theta}\hat{\phi}} = (A_{\phi,\theta} - A_{\theta,\phi}) \lambda_{\hat{\theta}}^\theta \lambda_{\hat{\phi}}^\phi \\
&= -\frac{3\mu [\cos \alpha \cos \theta + \sin \alpha \sin \theta \cos(\phi - \Omega t)]}{4m^3} \\
&\times \left[\ln \left(1 - \frac{2m}{r} \right) + \frac{2m}{r} \left(1 + \frac{m}{r} \right) \right], \quad (21)
\end{aligned}$$

$$\begin{aligned}
B_{\hat{\theta}} &= F_{\hat{\phi}\hat{r}} = -A_{\phi,r} \lambda_{\hat{\phi}}^\phi \lambda_{\hat{r}}^r \\
&= \frac{3\mu [\cos \alpha \sin \theta - \sin \alpha \cos \theta \cos(\phi - \Omega t)]}{4m^3} \\
&\times \left[\ln \left(1 - \frac{2m}{r} \right) + \frac{m}{r} \left(\left(1 - \frac{2m}{r} \right)^{-1} + 1 \right) \right] \\
&\times \left(1 - \frac{2m}{r} \right)^{1/2}, \quad (22)
\end{aligned}$$

$$\begin{aligned}
B_{\hat{\phi}} &= F_{\hat{r}\hat{\theta}} = A_{\theta,r} \lambda_{\hat{r}}^r \lambda_{\hat{\theta}}^\theta \\
&= \frac{3\mu \sin \alpha \sin(\phi - \Omega t)}{4m^3} \\
&\times \left[\ln \left(1 - \frac{2m}{r} \right) + \frac{m}{r} \left(\left(1 - \frac{2m}{r} \right)^{-1} + 1 \right) \right] \\
&\times \left(1 - \frac{2m}{r} \right)^{1/2}. \quad (23)
\end{aligned}$$

This is in agreement with [13],⁷ and also in agreement with [19] and [11] in the flat spacetime limit $m \rightarrow 0$ and in the alignment limit $\alpha \rightarrow 0$, respectively. In Fig. 3 are shown the magnetic field lines based on Eqs. (21)-(23), where we set $\phi - \Omega t = 0$.⁸ Note here the difference between the field lines in curved spacetime and flat spacetime: the blue curves represent the field lines in curved spacetime, with the general relativistic effect taken into account through $m = GM/c^2$ for the star of mass M , while the green curves represent the field lines in flat spacetime, in the limit $m \rightarrow 0$. The unity in the scale used for this graph is equivalent to the radius of the neutron star, $R_* \simeq 10^6$ cm.

⁶ The same results are obtained by directly transforming the magnetic field from the corotating frame to the reference frame by means of (16), (17) and (A15).

⁷ Our result is in agreement with their stationary vacuum magnetic field external to a misaligned magnetized rotator, which is obtained as part of the exterior solution of Maxwell's equations in the case of infinite electrical conductivity.

⁸ To be precise, the actual field lines are drawn by means of Eq. (61), where a collection of arbitrary constants chosen for the equation correspond to magnetic field lines as shown in Fig. 3.

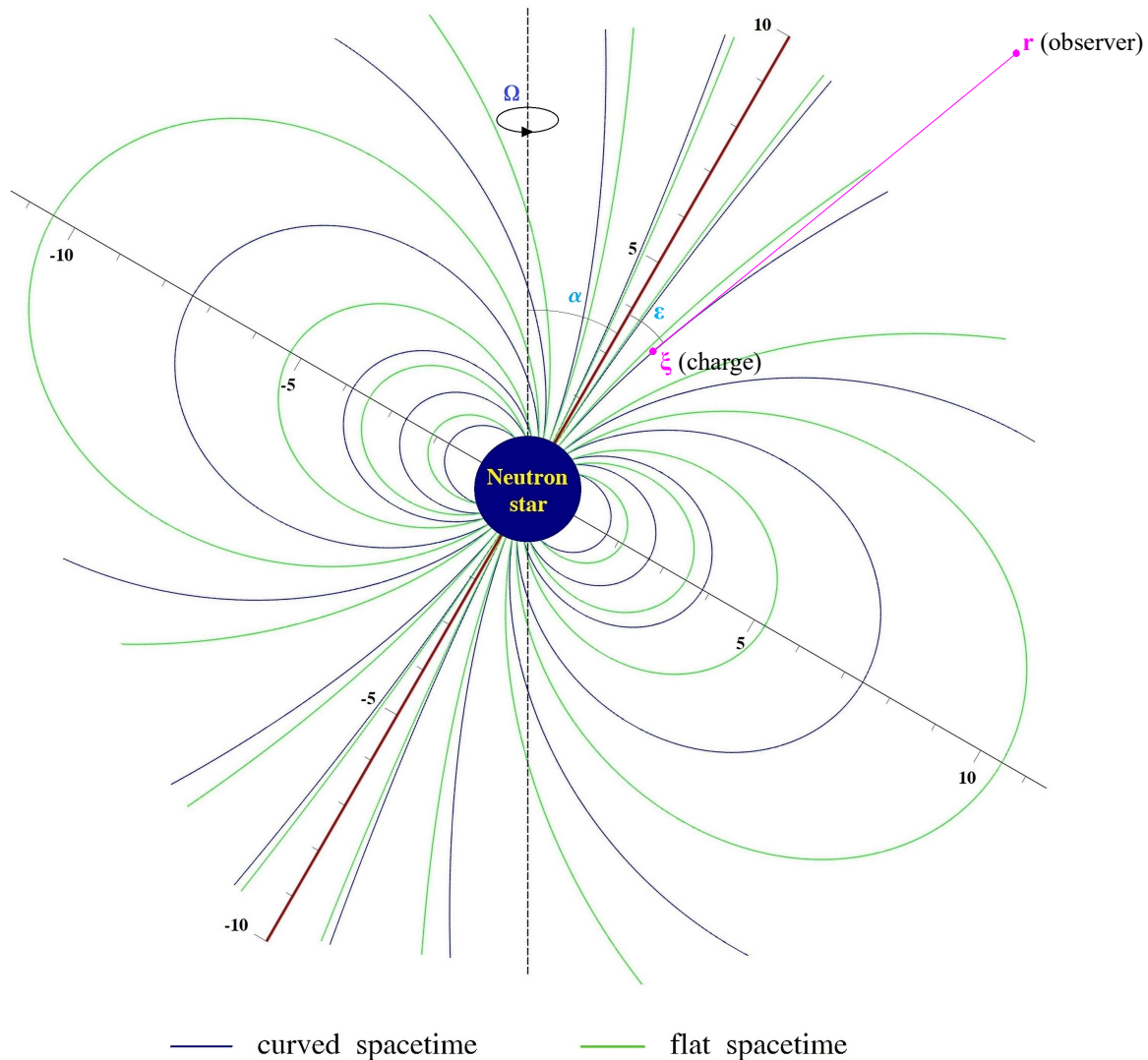


FIG. 3: The dipole magnetic field lines around the neutron star based on Eqs. (21)-(23), with $\phi - \Omega t$ set to be 0. The vertical dashed line (black) and the inclined solid line (red) represent the rotation axis and the magnetic axis, respectively. The field lines in curved spacetime (blue) are distinguished from those in flat spacetime (green). The scale of the unity in this graph is equivalent to the radius of the neutron star, $R_* \simeq 10^6$ cm. The magenta line connecting a source charge (ξ) and the observer (\mathbf{r}) illustrates a line of sight. While α (between the rotation axis and the magnetic axis) denotes the inclination angle, ε (between the magnetic axis and the line of sight) denotes the sight line impact angle.

III. PULSAR EMISSION AND EFFECTS OF OBLIQUITY

A. Radiative EM Fields and Pulsar Energetics

One of the most interesting features of an oblique rotator would be *low-frequency* EM radiation produced by its obliquely rotating magnetic dipole moment. We shall de-

note the magnetic dipole moment as $\mu(t)$, a time-varying vector. The vector potential due to $\mu(t)$, evaluated at the point \mathbf{r} at time t is (see [19])

$$\mathbf{A}(t, \mathbf{r}) = \nabla \times \left(\frac{\mu(t_{\text{R}})}{r} \right), \quad (24)$$

where $r = |\mathbf{r}|$ is the radial distance from the centre of the rotator, and $t_{\text{R}} \equiv t - r/c$ is the retarded time. Expanding

the right-hand side, we shall keep the term $\propto 1/r$, which will survive and give a radially outward Poynting vector in the far-field regime as will be shown below. This shall be termed the “radiative” potential [19]:

$$\mathbf{A}(t, \mathbf{r}) \sim \frac{\dot{\boldsymbol{\mu}}(t_{\text{R}}) \times \mathbf{e}_{\hat{r}}}{cr}, \quad (25)$$

where $\mathbf{e}_{\hat{r}} = \mathbf{r}/|\mathbf{r}|$ is the unit vector along the radial direction.⁹

The magnetic dipole moment $\boldsymbol{\mu}$ is *static* in the corotating frame and always points along the z' -axis:

$$\boldsymbol{\mu} = \mu \mathbf{e}_{z'}, \quad (26)$$

where $\mu = |\mu|$ is a constant. One can convert this expression into spherical coordinates in the inertial frame, which then becomes time-dependent:¹⁰

$$\begin{aligned} \boldsymbol{\mu} = \mu \left\{ & [\cos \alpha \cos \theta + \sin \alpha \sin \theta \cos(\phi - \Omega t)] \mathbf{e}_{\hat{r}} \right. \\ & + [-\cos \alpha \sin \theta + \sin \alpha \cos \theta \cos(\phi - \Omega t)] \mathbf{e}_{\hat{\theta}} \\ & \left. + [-\sin \alpha \sin(\phi - \Omega t)] \mathbf{e}_{\hat{\phi}} \right\}. \end{aligned} \quad (27)$$

Differentiation of Eq. (27) with respect to time t yields

$$\begin{aligned} \dot{\boldsymbol{\mu}} = \Omega \mu \sin \alpha \left[& \sin \theta \sin(\phi - \Omega t) \mathbf{e}_{\hat{r}} + \cos \theta \sin(\phi - \Omega t) \mathbf{e}_{\hat{\theta}} \right. \\ & \left. + \cos(\phi - \Omega t) \mathbf{e}_{\hat{\phi}} \right]. \end{aligned} \quad (28)$$

Substituting Eq. (28) into Eq. (25), we obtain the retarded potential:

$$A_{\hat{\theta}} = \frac{\Omega \mu \sin \alpha \cos(\phi - \Omega t_{\text{R}})}{cr}, \quad (29)$$

$$A_{\hat{\phi}} = -\frac{\Omega \mu \sin \alpha \cos \theta \sin(\phi - \Omega t_{\text{R}})}{cr}. \quad (30)$$

Then out of these the radiative EM fields can be finally determined:

$$B_{\hat{\theta}} = -A_{\hat{\phi},r} = \frac{\Omega^2 \mu \sin \alpha \cos \theta \cos(\phi - \Omega t_{\text{R}})}{c^2 r} + \mathcal{O}(r^{-2}), \quad (31)$$

$$B_{\hat{\phi}} = A_{\hat{\theta},r} = -\frac{\Omega^2 \mu \sin \alpha \sin(\phi - \Omega t_{\text{R}})}{c^2 r} + \mathcal{O}(r^{-2}), \quad (32)$$

⁹ The way our radiative potential is calculated here resembles a “semi-relativistic treatment” in Ref. [23], in the following senses: (i) the field $\mathbf{A}(t, \mathbf{r})$ radiates out in flat spacetime (to an observer far away from the source), (ii) the source $\boldsymbol{\mu}(t_{\text{R}})$ contains the general relativistic information about its local spacetime, which is strongly curved due to the mass of the neutron star.

¹⁰ The conversion can be achieved by means of Eqs. (A9)-(A12) in Appendix A.

and

$$E_{\hat{\theta}} = -A_{\hat{\theta},t} c^{-1} = -\frac{\Omega^2 \mu \sin \alpha \sin(\phi - \Omega t_{\text{R}})}{c^2 r}, \quad (33)$$

$$E_{\hat{\phi}} = -A_{\hat{\phi},t} c^{-1} = -\frac{\Omega^2 \mu \sin \alpha \cos \theta \cos(\phi - \Omega t_{\text{R}})}{c^2 r}, \quad (34)$$

where the terms of $\mathcal{O}(r^{-2})$ in Eqs. (31) and (32) can be disregarded in our analysis as they are too small to consider in the far-field regime.

Now, with the EM fields given by Eqs. (31)-(34) the Poynting vector reads

$$\begin{aligned} S_{\hat{r}} &= \frac{c}{4\pi} (E_{\hat{\theta}} B_{\hat{\phi}} - E_{\hat{\phi}} B_{\hat{\theta}}) \\ &= \frac{\mu^2 \Omega^4 \sin^2 \alpha}{4\pi c^3 r^2} \\ &\quad \times [\sin^2(\phi - \Omega t_{\text{R}}) + \cos^2 \theta \cos^2(\phi - \Omega t_{\text{R}})]. \end{aligned} \quad (35)$$

Then the power radiated by the EM fields can be evaluated as

$$\mathcal{P}_{\text{radiation}} = \int S_{\hat{r}} r^2 d\Omega = \frac{2\mu^2 \Omega^4 \sin^2 \alpha}{3c^3}, \quad (36)$$

where $d\Omega \equiv \sin \theta d\theta d\phi$ is a differential solid angle. From this, it should be noted that the power \mathcal{P} vanishes in the alignment limit $\alpha \rightarrow 0$: it implies that the “obliqueness” of our rotating star is responsible for radiation.

The above result can be applied to the well-known relation between pulsar radiation and rotational energy loss. That is, the radiation power $\mathcal{P}_{\text{radiation}}$ given by Eq. (36) is equated to the rate of loss of rotational kinetic energy $\dot{\mathcal{E}}_{\text{rotation}}$:

$$\mathcal{P}_{\text{radiation}} = -\dot{\mathcal{E}}_{\text{rotation}}, \quad (37)$$

where

$$\mathcal{E}_{\text{rotation}} = \frac{1}{2} J \Omega \simeq \frac{1}{5} M R_*^2 \Omega^2, \quad (38)$$

due to Eq. (4). In flat spacetime Eq. (37) leads to

$$\mu_{\text{flat}} \simeq \frac{\sqrt{3} c^{3/2} M^{1/2} R_*}{2\sqrt{5}\pi \sin \alpha} (P\dot{P})^{1/2}, \quad (39)$$

where $P = 2\pi/\Omega$ is the rotational period of the star. However, in curved spacetime, from Eq. (15) we may infer

$$\mu_{\text{curved}} = \left(1 - \frac{2m}{R_*}\right)^{1/2} \mu_{\text{flat}}, \quad (40)$$

which implies $\mu_{\text{curved}} \rightarrow \mu_{\text{flat}} = \pi R_*^2 I$ in the limit $m \rightarrow 0$ for the current loop model as presented in Section II B 2. Then using Eqs. (39) and (40), we may express

$$\mu_{\text{curved}} \simeq \frac{\sqrt{3} c^{3/2} M^{1/2} R_* \left(1 - \frac{2m}{R_*}\right)^{1/2}}{2\sqrt{5}\pi \sin \alpha} (P\dot{P})^{1/2}. \quad (41)$$

Now, by Eq. (16) we find the magnetic field strength at

the polar cap to be

$$B_* \equiv B_{\hat{r}}(r = R_*, \theta' = 0) \\ = -\frac{3\mu_{\text{curved}}}{4m^3} \left[\ln \left(1 - \frac{2m}{R_*} \right) + \frac{2m}{R_*} \left(1 + \frac{m}{R_*} \right) \right]. \quad (42)$$

Inserting Eq. (41) into Eq. (42), we finally obtain

$$B_{* \text{ curved}} \simeq -\frac{3\sqrt{3} c^{3/2} M^{1/2} R_* \left[\ln \left(1 - \frac{2m}{R_*} \right) + \frac{2m}{R_*} \left(1 + \frac{m}{R_*} \right) \right] \left(1 - \frac{2m}{R_*} \right)^{1/2}}{8\sqrt{5}\pi m^3 \sin \alpha} (P\dot{P})^{1/2}. \quad (43)$$

This provides a general relativistic estimate of B_* as $m = GM/c^2$ takes into account the effect of gravitation.

In the limit $m \rightarrow 0$, Eq. (43) reduces to the expression for B_* in flat spacetime [24]:

$$B_{* \text{ flat}} \simeq \frac{\sqrt{3} c^{3/2} M^{1/2}}{\sqrt{5}\pi R_*^2 \sin \alpha} (P\dot{P})^{1/2}. \quad (44)$$

Taking the ratio between the right-hand sides of Eqs. (43) and (44), we find the general relativistic factor for the estimate of B_* :

$$\text{GR factor} = \frac{B_{* \text{ curved}}}{B_{* \text{ flat}}} \\ = -\frac{3R_*^3 \left[\ln \left(1 - \frac{2m}{R_*} \right) + \frac{2m}{R_*} \left(1 + \frac{m}{R_*} \right) \right] \left(1 - \frac{2m}{R_*} \right)^{1/2}}{8m^3}, \quad (45)$$

which tends to 1 in the flat spacetime limit $m \rightarrow 0$. For example, the Crab pulsar (PSR B0531+21) has the radius $R_* \simeq 10^6$ cm and $M \simeq 1.4 M_\odot$, with observed data $P = 0.0333$ s, $\dot{P} = 4.21 \times 10^{-13}$. Then $m = GM/c^2 \simeq 2.065 \times 10^5$ cm, and by Eqs. (43), (44) and (45) we have

$$B_{* \text{ curved}} \sin \alpha \simeq 9.0 \times 10^{12} \text{ G}, \quad (46)$$

and

$$B_{* \text{ flat}} \sin \alpha \simeq 8.0 \times 10^{12} \text{ G}, \quad (47)$$

with

$$\text{GR factor} \simeq 1.12. \quad (48)$$

That is, the general relativistic effect increases the estimate of B_* by 12%. The classical result (47) is commonly used in observational studies of various properties of the Crab pulsar; e.g., in [25] it is assumed that a field strength

at the magnetic poles is about 7.6×10^{12} G. However, a correction due to the GR-induced enhancement would not be significant as it keeps the estimate still within the same order of magnitude. There are other things to take into consideration, such as the dust and gas interacting with the pulsar in the surrounding nebula, which would give rise to torques that contribute to slowing down the pulsar's spin [24].

B. Pulsar Radio Emission

1. Curvature Radiation

As one of the possible mechanisms for pulsar radio emission, curvature radiation can be discussed. It is emitted by a charged particle moving from the region near the polar cap of our neutron star along a dipole magnetic field line close to the magnetic axis, and received by an observer who is far away from the star. The radiation can be obtained from the Liénard–Wiechert potential. For a moving point charge q at position ξ , it is evaluated by an observer at the point \mathbf{r} at time t as:

$$\mathbf{A}(t, \mathbf{r}) = \frac{q\dot{\xi}(t_{\text{R}})}{c \left(1 - \frac{\dot{\xi}(t_{\text{R}})}{c} \cdot \mathbf{n} \right) |\mathbf{r} - \xi(t_{\text{R}})|}, \quad (49)$$

where $\mathbf{n} = (\mathbf{r} - \xi(t_{\text{R}})) / |\mathbf{r} - \xi(t_{\text{R}})|$ is the unit vector pointing in the direction from the charge to the field point, and $t_{\text{R}} \equiv t - |\mathbf{r} - \xi(t_{\text{R}})|/c$ is the retarded time, and the overdot denotes differentiation with respect to t_{R} . A simple configuration for this emission mechanism is illustrated in Fig. 3: the observer's line of sight, i.e., the line connecting the two points ξ and \mathbf{r} is represented by the purple dashed line.

In this mechanism, a charge is assumed to move along a

magnetic field line; therefore, its trajectory ξ is identified with the field line. Then its velocity is tangent to the field line at the point ξ and can be written as

$$\dot{\xi} = \dot{\xi} \hat{\mathbf{v}} = \beta c \hat{\mathbf{B}}(\xi), \quad (50)$$

where $\dot{\xi} = \beta c = \text{const.}$, and $\hat{\mathbf{v}} \equiv \hat{\mathbf{B}}(\xi) = \mathbf{B}(\xi) / |\mathbf{B}(\xi)|$ denotes the unit vector along which the radiation pulse propagates: it also coincides with $\mathbf{n} = (\mathbf{r} - \xi) / |\mathbf{r} - \xi|$, the unit vector along the line of sight.

In the same plane where a magnetic field line belongs, the acceleration of a charge that moves along the field line can be expressed as

$$\ddot{\xi} = \beta c \dot{\hat{\mathbf{v}}} = \beta c \dot{\hat{\mathbf{B}}}(\xi) = \ddot{\xi} \hat{\mathbf{a}} = \beta c \left| \dot{\hat{\mathbf{B}}}(\xi) \right| \left(\frac{\dot{\hat{\mathbf{B}}}(\xi)}{\left| \dot{\hat{\mathbf{B}}}(\xi) \right|} \right), \quad (51)$$

where $\ddot{\xi} = \beta c \left| \dot{\hat{\mathbf{B}}}(\xi) \right|$, and $\hat{\mathbf{a}} \equiv \dot{\hat{\mathbf{B}}}(\xi) / \left| \dot{\hat{\mathbf{B}}}(\xi) \right|$ denotes the unit vector along which the radiation pulse is polarized. From $\dot{\xi} = \beta c = \text{const.}$, one can easily check the orthogonality, $\dot{\xi} \cdot \ddot{\xi} = 0$.

Now, in the corotating frame, magnetic field lines are static, and therefore the description of motion of a charge along a field line would be much simpler than in the inertial frame. By means of Eqs. (16), (17), (50) and (51) the velocity and the acceleration are expressed respectively as

$$\dot{\xi} = \beta c \hat{\mathbf{v}}; \text{ with } \hat{\mathbf{v}} = \frac{B_{\hat{r}}(\xi) \mathbf{e}_{\hat{r}} + B_{\hat{\theta}'}(\xi) \mathbf{e}_{\hat{\theta}'}}{\sqrt{B_{\hat{r}}^2(\xi) + B_{\hat{\theta}'}^2(\xi)}}, \quad (52)$$

and

$$\ddot{\xi} = \frac{\beta^2 c^2}{\rho} \hat{\mathbf{a}}; \text{ with } \hat{\mathbf{a}} = \frac{-B_{\hat{\theta}'}(\xi) \mathbf{e}_{\hat{r}} + B_{\hat{r}}(\xi) \mathbf{e}_{\hat{\theta}'}}{\sqrt{B_{\hat{r}}^2(\xi) + B_{\hat{\theta}'}^2(\xi)}}, \quad (53)$$

where ρ is the curvature radius of the charge's trajectory along a magnetic field line, which is defined through Eqs. (58)-(62) below.

The trajectory of a source charge moving along a magnetic field line can be expressed by

$$\xi_s = r_s \mathbf{e}_{\hat{r}} \text{ at } \theta'_s, \quad (54)$$

where the subscript "s" denotes the source charge: the trajectory is equivalent to the field line given by Eqs. (16) and (17) defined at the location of the source charge (r_s, θ'_s) in the corotating frame. Further, the velocity and the acceleration of the source charge can be expressed using (52) and (53): by means of Eqs. (16) and (17), we have

$$\dot{\xi}_s = \beta c \hat{\mathbf{v}}; \text{ with } \hat{\mathbf{v}} = \frac{-g(r_s) \mathbf{e}_{\hat{r}} + \tan \theta'_s \mathbf{e}_{\hat{\theta}'}}{\sqrt{g^2(r_s) + \tan^2 \theta'_s}}, \quad (55)$$

and

$$\ddot{\xi}_s = \frac{\beta^2 c^2}{\rho} \hat{\mathbf{a}}; \text{ with } \hat{\mathbf{a}} = \frac{-\tan \theta'_s \mathbf{e}_{\hat{r}} - g(r_s) \mathbf{e}_{\hat{\theta}'}}{\sqrt{g^2(r_s) + \tan^2 \theta'_s}}, \quad (56)$$

where

$$g(r) \equiv \frac{\ln\left(1 - \frac{2m}{r}\right) + \frac{2m}{r} \left(1 + \frac{m}{r}\right)}{\left[\ln\left(1 - \frac{2m}{r}\right) + \frac{m}{r} \left(\left(1 - \frac{2m}{r}\right)^{-1} + 1\right)\right] \left(1 - \frac{2m}{r}\right)^{1/2}}. \quad (57)$$

Viewed in the inertial frame, $\hat{\mathbf{v}}$ and $\hat{\mathbf{a}}$ in Eqs. (55) and (56) can be set to lie in the $\hat{r}\hat{\theta}$ -plane. A magnetic field line can be confined to this plane via Eq. (A15) and by defining Eqs. (21)-(23) at $\xi_s = (r_s, \theta_s, \phi_s)$ with $\phi_s = \Omega t_R$. Further, we have the magnetic colatitude being reduced to $\theta'_s = \theta_s - \alpha$ in the plane via Eq. (10). In view of Fig. 3, it should be noted that the trajectory ξ_s , the velocity $\dot{\xi}_s$ and the acceleration $\ddot{\xi}_s$ of a source charge may describe its motion either in curved spacetime or in flat spacetime. That is, the charge moves along the magnetic field lines in blue in curved spacetime, with the general relativistic effect taken into account in Eqs. (21)-(23) through $m = GM/c^2$ for a neutron star of mass M , while it moves along the magnetic field lines in green in flat spacetime, in the limit $m \rightarrow 0$. Notable differences between the cases of curved and flat spacetimes are the directions of $\dot{\xi}_s$ and $\ddot{\xi}_s$, which can be easily checked from Eqs. (55) and (56). However, the most significant distinction between the two cases is characterized by ρ , the curvature radius of the charge's trajectory: the general relativistic effect, which is due to strong gravity in the pulsar magnetosphere, causes the curvature radius to shrink and thence the acceleration to increase since $\left| \ddot{\xi}_s \right| = \beta^2 c^2 / \rho$ according to Eq. (56).¹¹

The curvature radius ρ in the general relativistic context can be defined from an infinitesimal path of a charge moving along a magnetic field line in curved spacetime. Considering the charge's trajectory as described by Eq. (54), one can write down the infinitesimal path:

$$d\mathbf{l} = dr'_s \mathbf{e}_{\hat{r}} + d\theta'_s \mathbf{e}_{\hat{\theta}'}, \\ = \left(1 - \frac{2m}{r_s}\right)^{-1/2} dr_s \mathbf{e}_{\hat{r}} + r_s d\theta'_s \mathbf{e}_{\hat{\theta}'}. \quad (58)$$

¹¹ In contrast to this, the general relativistic effect causes the direction of the velocity to change but not its magnitude, $\left| \dot{\xi} \right| = \beta c$ according to Eq. (55).

This is defined in a local Lorentz frame by means of the tetrad (18); that is, with $d\hat{r} = dr (\lambda_r^r)^{-1}$ and $d\theta' = d\theta' (\lambda_{\theta'}^{\theta'})^{-1}$ being defined at $\xi_s = (r_s, \theta'_s)$. The infinitesimal arc length along the field line is then given by

$$dl = |d\mathbf{l}| = r_s d\theta'_s \left[1 + r_s^{-2} \left(1 - \frac{2m}{r_s} \right)^{-1} \left(\frac{B_r(\xi_s)}{B_{\theta'}(\xi_s)} \right)^2 \right]^{1/2}. \quad (59)$$

Here the second term inside the square brackets is due to the differential equation [12, 26]:

$$\frac{dr_s}{d\theta'_s} = \frac{B_r(\xi_s)}{B_{\theta'}(\xi_s)}, \quad (60)$$

where $B_r(\xi_s)$ and $B_{\theta'}(\xi_s)$ mean $B_{\hat{r}}(\lambda_r^r)^{-1}$ and $B_{\hat{\theta}'}(\lambda_{\theta'}^{\theta'})^{-1}$ defined at $\xi_s = (r_s, \theta'_s)$, respectively, by means of Eqs. (16), (17) and (18). A solution to Eq. (60) is a curve

$$A_{\phi'}(\xi_s) = \text{const.}, \quad (61)$$

where $A_{\phi'}(\xi_s)$ is given by Eq. (14) defined at $\xi_s = (r_s, \theta'_s)$.¹² Out of Eq. (59) one can finally define the curvature radius of a charge's trajectory along a magnetic field line [12]:

$$\rho \equiv \frac{dl}{d\theta'_s} = r_s \left[1 + \left(\frac{B_r(\xi_s)}{B_{\theta'}(\xi_s)} \right)^2 \right]^{1/2}. \quad (62)$$

Having Eqs. (16) and (17) defined at $\xi_s = (r_s, \theta'_s)$, the curvature radius is evaluated from Eq. (62):

$$\rho = r_s [1 + g^2(r_s) \cot^2 \theta'_s]^{1/2}, \quad (63)$$

where $g(r)$ refers to Eq. (57). In the flat spacetime limit $m \rightarrow 0$, we have $g(r_s) \rightarrow -2$, and thence

$$\rho = r_s [1 + 4 \cot^2 \theta'_s]^{1/2}. \quad (64)$$

Obviously, the difference between Eqs. (63) and (64) shows the general relativistic effect due to gravity in the pulsar magnetosphere: $\rho_{\text{curved}} \leq \rho_{\text{flat}}$ as $g^2(r_s) \leq 4$.¹³

¹² The solution can easily be verified: $A_{\phi',r}(\xi_s) dr_s + A_{\phi',\theta'}(\xi_s) d\theta'_s = 0 \Leftrightarrow -B_{\theta'}(\xi_s) dr_s + B_r(\xi_s) d\theta'_s = 0$.

¹³ For example, for curvature radiation from the pulsar PSR J1828-1101 (see Section III B 2), the emission heights of source charges are estimated to be around 35 to 45 km, relative to the center of the neutron star [10]. Then for $\theta'_s \ll 1$, we have the ratio $\rho_{\text{curved}}/\rho_{\text{flat}} \approx |g(r_s)|/2 \approx 0.96$ to 0.97, where $r_s \simeq 3.5R_*$ to $4.5R_* \simeq 14m$ to $18m$.

From Eq. (50) and the definition of the curvature radius, we find

$$\dot{\xi}_s = \beta c \hat{\mathbf{v}} = \dot{l} \hat{\mathbf{v}} = \rho \dot{\theta}'_s \hat{\mathbf{v}}. \quad (65)$$

From this the frequency of radiation by a moving charge is obtained:

$$\omega_o \equiv \dot{\theta}'_s = \frac{\beta c}{\rho}. \quad (66)$$

However, for a source charge moving near the speed of light, i.e., $\gamma = (1 - \beta^2)^{-1/2} \gg 1$, we take into consideration the *relativistic beaming* effect, and the characteristic frequency for the curvature radiation should be expressed as [27]

$$\omega_c = \frac{3}{2} \gamma^3 \frac{\beta c}{\rho}. \quad (67)$$

Out of the potential (49), the electric field is derived:

$$\mathbf{E}(t, \mathbf{r}) = \frac{q\mathbf{n} \times \left[\left(\mathbf{n} - \frac{\dot{\xi}(t_R)}{c} \right) \times \frac{\ddot{\xi}(t_R)}{c} \right]}{c \left(1 - \frac{\dot{\xi}(t_R)}{c} \cdot \mathbf{n} \right)^3 |\mathbf{r} - \xi(t_R)|} + \frac{q\mathbf{n} \left(\mathbf{n} - \frac{\dot{\xi}(t_R)}{c} \right)}{\gamma^2 \left(1 - \frac{\dot{\xi}(t_R)}{c} \cdot \mathbf{n} \right)^3 |\mathbf{r} - \xi(t_R)|^2}. \quad (68)$$

Here the first term $\sim |\mathbf{r} - \xi(t_R)|^{-1}$ pertains to *radiation* by a moving charge, requiring the charge acceleration $\ddot{\xi}$, whereas the second term $\sim |\mathbf{r} - \xi(t_R)|^{-2}$ refers to the *static* part of the electric field of the charge and will be disregarded in our analysis.

For a distant observer, i.e., $|\mathbf{r}| \gg |\xi_s|$, we have $\mathbf{n} = (\mathbf{r} - \xi_s) / |\mathbf{r} - \xi_s| \approx \hat{\mathbf{r}} = \mathbf{r} / |\mathbf{r}|$, and therefore from (68) the electric field of radiation can be expressed as [28–30]

$$\mathbf{E}(t, \mathbf{r}) \approx \frac{q\hat{\mathbf{r}} \times \left[\left(\hat{\mathbf{r}} - \frac{\dot{\xi}_s(t_R)}{c} \right) \times \frac{\ddot{\xi}_s(t_R)}{c} \right]}{c \left(1 - \frac{\dot{\xi}_s(t_R)}{c} \cdot \hat{\mathbf{r}} \right)^3 |\mathbf{r} - \xi_s(t_R)|}, \quad (69)$$

where

$$\xi_s = \rho (\sin \vartheta, 0, \cos \vartheta), \quad (70)$$

$$\dot{\xi}_s = \beta c (\cos \vartheta, 0, -\sin \vartheta), \quad (71)$$

$$\ddot{\xi}_s = \frac{\beta^2 c^2}{\rho} (-\sin \vartheta, 0, -\cos \vartheta), \quad (72)$$

refer to the trajectory, velocity and acceleration of a source charge, respectively in the corotating frame given by (54)-(56), being expressed in a Cartesian frame specially chosen for computational convenience, and

$$\hat{\mathbf{r}} = (\cos \varphi, \sin \varphi, 0). \quad (73)$$

Here the motion of the charge along the field line is parametrized by t_R via the polar angle ϑ , i.e., $\vartheta = \beta ct_R/\rho$, whereas the observational direction is parametrized by the azimuthal angle φ . A simple geometrical configuration for curvature radiation viewed in this Cartesian frame is illustrated in Fig. 4. In Appendix B the technical details are provided regarding how the Cartesian expressions for ξ_s , $\dot{\xi}_s$ and $\ddot{\xi}_s$ above can be obtained through the coordinate transformations of the initial spherical polar representations (54)-(56).

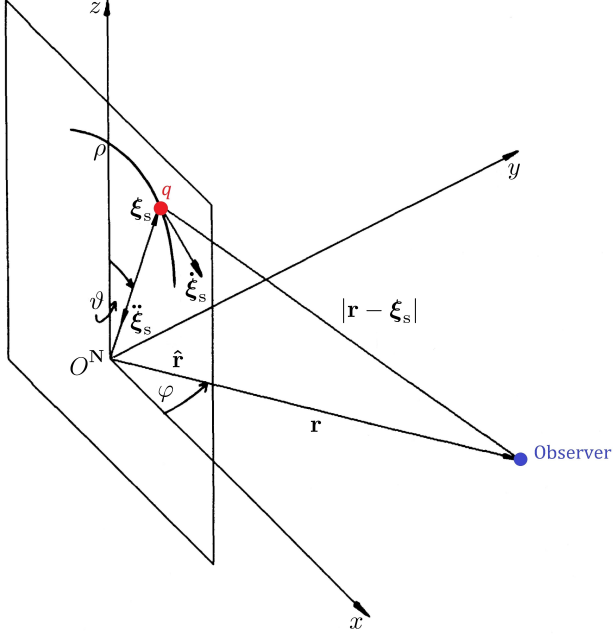


FIG. 4: A geometrical configuration for curvature radiation viewed in a specially chosen Cartesian frame. Note that the frame is centred at a new origin O^N (see Appendix B for technical details). (Credit: Gil and Snakowski [30]; reproduced with some modifications.)

2. Pulse Profiles

Following [28–31], one can express Stokes parameters out of the radiation field (69), which describe polarization

properties of the curvature radiation discussed above:

$$\begin{aligned} I &= \tilde{E}_{\parallel}^* \tilde{E}_{\parallel} + \tilde{E}_{\perp}^* \tilde{E}_{\perp} \\ &= \mathcal{E}_o^2 \omega^2 \left[(\delta^2 + \varphi^2)^2 K_{2/3}^2 \left(\frac{\omega}{3\omega_o} (\delta^2 + \varphi^2)^{3/2} \right) \right. \\ &\quad \left. + \varphi^2 (\delta^2 + \varphi^2)^2 K_{1/3}^2 \left(\frac{\omega}{3\omega_o} (\delta^2 + \varphi^2)^{3/2} \right) \right], \end{aligned} \quad (74)$$

$$\begin{aligned} Q &= \tilde{E}_{\parallel}^* \tilde{E}_{\perp} - \tilde{E}_{\perp}^* \tilde{E}_{\parallel} \\ &= \mathcal{E}_o^2 \omega^2 \left[(\delta^2 + \varphi^2)^2 K_{2/3}^2 \left(\frac{\omega}{3\omega_o} (\delta^2 + \varphi^2)^{3/2} \right) \right. \\ &\quad \left. - \varphi^2 (\delta^2 + \varphi^2)^2 K_{1/3}^2 \left(\frac{\omega}{3\omega_o} (\delta^2 + \varphi^2)^{3/2} \right) \right], \end{aligned} \quad (75)$$

$$\begin{aligned} U &= \tilde{E}_{\parallel}^* \tilde{E}_{\perp} + \tilde{E}_{\perp}^* \tilde{E}_{\parallel} \\ &= 2 \cos \psi \mathcal{E}_o^2 \omega^2 \varphi (\delta^2 + \varphi^2)^2 \\ &\quad \times K_{2/3} \left(\frac{\omega}{3\omega_o} (\delta^2 + \varphi^2)^{3/2} \right) K_{1/3} \left(\frac{\omega}{3\omega_o} (\delta^2 + \varphi^2)^{3/2} \right), \end{aligned} \quad (76)$$

$$\begin{aligned} V &= -i (\tilde{E}_{\parallel}^* \tilde{E}_{\perp} - \tilde{E}_{\perp}^* \tilde{E}_{\parallel}) \\ &= 2 \sin \psi \mathcal{E}_o^2 \omega^2 \varphi (\delta^2 + \varphi^2)^2 \\ &\quad \times K_{2/3} \left(\frac{\omega}{3\omega_o} (\delta^2 + \varphi^2)^{3/2} \right) K_{1/3} \left(\frac{\omega}{3\omega_o} (\delta^2 + \varphi^2)^{3/2} \right), \end{aligned} \quad (77)$$

where \tilde{E}_{\parallel} and \tilde{E}_{\perp} denote the Fourier transform $\tilde{\mathbf{E}}(\omega) = \int_{-\infty}^{\infty} \mathbf{E}(t) \exp(i\omega t) dt$, decomposed as $\tilde{E}_{\parallel}(\omega) \mathbf{e}_z + \tilde{E}_{\perp}(\omega) \mathbf{e}_y$ in the Cartesian frame as illustrated in Fig. 4, and $*$ means the complex conjugate, and $\mathcal{E}_o = q\omega_o / (2\sqrt{3}\pi^2 cr)$ with ω_o being defined by Eq. (66), and $\delta \equiv \gamma^{-1} = (1 - \beta^2)^{1/2} \ll 1$ is the half-angle of the beam emission, and $K_{1/3}$ and $K_{2/3}$ denote the modified Bessel functions of the second kind, and $\psi = \psi_{\parallel} - \psi_{\perp}$ is the phase difference between the two components of the electric field having different initial phases; $E_{\parallel}(t) \sim \exp[i(\omega t + \psi_{\parallel})]$ and $E_{\perp}(t) \sim \exp[i(\omega t + \psi_{\perp})]$. With regard to the polarization state, I is a measure of the total intensity, Q and U jointly describe the linear polarization, and V describes the circular polarization of the curvature radiation. We plot these parameters as functions of the phase angle φ to simulate the pulse profiles of pulsar radio emission theoretically.

Apart from the characteristic frequency ω_c given by (67), one can define the *peak* frequency ω_p of the intensity I at the center of the beam [30]:

$$\left. \frac{\partial I(\omega, \varphi)}{\partial \omega} \right|_{\varphi=0, \omega=\omega_p} = 0. \quad (78)$$

Then using Eq. (74), it turns out

$$\omega_p \approx 1.251 \gamma^3 \omega_o = 1.251 \gamma^3 \frac{\beta c}{\rho}, \quad (79)$$

which is of the same order as the characteristic frequency ω_c given by (67). However, at $\varphi = 0$, the argument of the modified Bessel functions in (74)-(77) above becomes

$$\frac{\delta^3 \omega}{3\omega_o} = \frac{\omega}{3\gamma^3 \omega_o} \approx 0.417 \frac{\omega}{\omega_p}. \quad (80)$$

Hence, the ratio $\omega/\omega_p \approx 1.2\omega/\omega_c$ will play an important role in determining the general features of the pulse profiles of the Stokes parameters plotted from (74)-(77) above.

Further, the pulse profiles can be expressed as functions of the rotation phase ϕ rather than the magnetic azimuthal phase φ . To this end, one substitutes into Eqs. (74)-(77) the conversion

$$\begin{aligned} \varphi &= \arctan \left(\frac{\sin \theta \sin \phi}{\sin \alpha \cos \theta - \cos \alpha \sin \theta \cos \phi} \right) \\ &\approx \arctan \left(\frac{\sin(\alpha + \varepsilon) \sin \phi}{\sin \alpha \cos(\alpha + \varepsilon) - \cos \alpha \sin(\alpha + \varepsilon) \cos \phi} \right) \\ &\quad + \mathcal{O}((\theta - (\alpha + \varepsilon))), \end{aligned} \quad (81)$$

$$\begin{aligned} \rho &= r_s \left[1 + \frac{g^2(r_s) [\cos \alpha \cos \theta + \sin \alpha \sin \theta \cos \phi]^2}{1 - [\cos \alpha \cos \theta + \sin \alpha \sin \theta \cos \phi]^2} \right]^{1/2} \\ &\approx r_s \left[1 + \frac{g^2(r_s) [\cos \alpha \cos(\alpha + \varepsilon) + \sin \alpha \sin(\alpha + \varepsilon) \cos \phi]^2}{1 - [\cos \alpha \cos(\alpha + \varepsilon) + \sin \alpha \sin(\alpha + \varepsilon) \cos \phi]^2} \right]^{1/2} + \mathcal{O}((\theta - (\alpha + \varepsilon))), \end{aligned} \quad (82)$$

where $g(r)$ refers to Eq. (57): $g^2(r_s) \leq 4$ with $g(r_s) \rightarrow -2$ in the flat spacetime limit $m \rightarrow 0$. Here again, the approximation in the second line is based upon radiation emitted from a single source charge at $\theta_s = \alpha + \varepsilon$ on a magnetic field line.

The technical details regarding the conversion (81) and the curvature radius (82) are presented in Appendix C.

Example: PSR J1828-1101

The pulsar PSR J1828-1101 is known to show ‘inter-pulse’ emission, which is nearly 180° apart from its main

where the approximation in the second line is based upon radiation emitted from a single source charge at $\theta_s = \alpha + \varepsilon$ on a magnetic field line, with α and ε denoting the inclination angle and the sight line impact angle [32], respectively (see Fig. 3 for illustration of α and ε).¹⁴

The pulse profiles (74)-(77) are dependent upon the curvature radius ρ through ω_o given by Eq. (66). Hence, along with the conversion (81) above, the curvature radius as given by Eq. (63) should also be rewritten such that its dependence on the rotation phase ϕ is retrieved. It is expressed as

pulse emission in rotation phase, and hence is close to an orthogonal rotator with an inclination angle near 90° [10]. Besides, this pulsar has a very important property that we can exploit for our general relativistic analysis of pulsar radio emission: its emission heights for both main and interpulse emissions are fairly low; viz., a few times the radius of the neutron star, at which gravity has a significant effect on the pulse profiles. In order to compare theoretical and observed pulse profiles for this source, we obtained the full-polarization pulse profiles observed by the Parkes radio telescope at 1.4 GHz and published by [10].¹⁵ The data are summarized in Figs. 5 and 6.

The pulse profiles for the emission from this pulsar can be plotted out of the Stokes parameters $S = \{I, Q, U, V\}$ given by Eqs. (74)-(77) against the rotation phase ϕ by means of Eqs. (66), (81) and (82). These Stokes param-

¹⁴ Later, the pulse profile curves as shown in Figs. 5 and 6 are plotted with an assumption of radiation emitted by a bunch of charges rather than a single charge. Then, for a charge bunch centred at $\theta = \alpha + \varepsilon$, the contribution from the term $\mathcal{O}((\theta - (\alpha + \varepsilon)))$ would not be negligible; in fact, the Gaussian modulation of this over θ will cause the pulse profile curves to shift upward or downward.

¹⁵ Data were provided by S. Johnston in private communication.

eters are expressed using the basis of linearly polarized waves [33]:

$$\mathbf{e}_{\parallel} = \begin{bmatrix} 1 \\ 0 \end{bmatrix}; \quad \mathbf{e}_{\perp} = \begin{bmatrix} 0 \\ 1 \end{bmatrix}, \quad (83)$$

where \mathbf{e}_{\parallel} and \mathbf{e}_{\perp} denote linear polarization in the directions parallel and perpendicular to the plane of motion of the charge, respectively, as illustrated in Fig. 4. However, the Stokes parameters can also be expressed using the basis $\{\mathbf{e}_1, \mathbf{e}_2\} = \{\mathbf{e}_{\perp}, \mathbf{e}_{\parallel}\}$, i.e., with the basis vectors swapped. In this basis the Stokes parameters $S' = \{I', Q', U', V'\}$ read

$$I' = \tilde{E}_1^* \tilde{E}_1 + \tilde{E}_2^* \tilde{E}_2 = \tilde{E}_{\perp}^* \tilde{E}_{\perp} + \tilde{E}_{\parallel}^* \tilde{E}_{\parallel} = I, \quad (84)$$

$$Q' = \tilde{E}_1^* \tilde{E}_1 - \tilde{E}_2^* \tilde{E}_2 = \tilde{E}_{\perp}^* \tilde{E}_{\perp} - \tilde{E}_{\parallel}^* \tilde{E}_{\parallel} = -Q, \quad (85)$$

$$U' = \tilde{E}_1^* \tilde{E}_2 + \tilde{E}_1 \tilde{E}_2^* = \tilde{E}_{\perp}^* \tilde{E}_{\parallel} + \tilde{E}_{\perp} \tilde{E}_{\parallel}^* = U, \quad (86)$$

$$V' = -i \left(\tilde{E}_1^* \tilde{E}_2 - \tilde{E}_1 \tilde{E}_2^* \right) = -i \left(\tilde{E}_{\perp}^* \tilde{E}_{\parallel} - \tilde{E}_{\perp} \tilde{E}_{\parallel}^* \right) = -V, \quad (87)$$

where the third and the fourth equalities are consistent with the phase difference, $\cos(\psi_1 - \psi_2) = \cos(\psi_{\perp} - \psi_{\parallel}) = \cos\psi$ and $\sin(\psi_1 - \psi_2) = \sin(\psi_{\perp} - \psi_{\parallel}) = -\sin\psi$, in comparison with Eqs. (76) and (77), respectively.

Further, one can consider the pulsar emission as coherent curvature radiation by a bunch of charged particles, rather than single-particle radiation. Taking this into consideration, our pulse profiles can be modeled using a Gaussian modulation function [30, 32, 34]. One can define new Stokes parameters $\mathcal{S} = \{\mathcal{I}, \mathcal{Q}, \mathcal{U}, \mathcal{V}\}$ as

$$\mathcal{S}(\lambda\phi) \equiv \int S' f(\theta_*, \phi_*) d\theta_* d\phi_*, \quad (88)$$

where λ is a free scaling factor to resize the rotation phase ϕ ¹⁶, and $S' = \{I', Q', U', V'\}$ refers to Eqs. (84)-(87), and

$$f(\theta_*, \phi_*) = \frac{\exp\left(-\frac{(\theta_* - \theta_o)^2}{\sigma_{\theta}^2}\right) \exp\left(-\frac{(\phi_* - \phi_o)^2}{\sigma_{\phi}^2}\right)}{2\pi\sigma_{\theta}\sigma_{\phi}\tau} \quad (89)$$

is the modulation function with σ_{θ} and σ_{ϕ} being the angular spread over θ and ϕ , respectively, covering a patch

¹⁶ We absorbed two effects in the factor λ : (1) For a distant observer of the radiation from a collimated bunch of mono-energetic charges with Lorentz factor γ , the effective phase angle is $\gamma \sin\phi$ (e.g., [33]), corresponding to $\gamma\phi$ in small-angle approximation; (2) a distant observer receives emission from an extended area on the surface of the neutron star, which leads to a spread of the pulse over a range of phase angles.

over a segment of a bundle of pulsar magnetic field lines, and (θ_o, ϕ_o) defining the peak location of the function, equivalent to the centre of a charge bunch, and τ being a tuning factor to adjust the peak height. Now, with consideration of (81) and (82) in regard to (84)-(87), the expression (88) can be approximated as¹⁷

$$\mathcal{S}(\lambda\phi) \approx \int [S'(\phi - \phi_*) + \mathcal{O}((\theta - \theta_*))] f(\theta_*, \phi_*) d\theta_* d\phi_*. \quad (90)$$

In Fig. 5 are presented the pulse profiles for the “main pulse” of curvature radiation from PSR J1828-1101. Fig. 5a shows the plots of I (black), Q (red), U (green) and V (blue) created based on the actual data obtained from observations at 1.4 GHz. Corresponding to this, Fig. 5b shows our theoretical plots of \mathcal{I} (black), \mathcal{Q} (red), \mathcal{U} (green) and \mathcal{V} (blue) for the emission by a Gaussian particle bunch in curved (solid line) and flat (dashed line) spacetimes: they are modeled with the emission height $r_s \simeq 3.5 \times 10^6$ cm; the inclination angle $\alpha = 82^\circ.7$; the sight line impact angle $\varepsilon = 7^\circ.3$; the phase $\psi = 0^\circ$; the angular spread $\sigma_{\phi} = 0^\circ.17$; the peak location $\phi_o = 2^\circ$; the tuning factor $\tau = 1$; the scaling factor $\lambda = \frac{1}{10}$ (which matches the model pulse width to the observed width), for the neutron star mass $M \simeq 1.4 M_{\odot}$ ($m = GM/c^2 \simeq 2.065 \times 10^5$ cm); the Lorentz factor $\gamma = 400$; the observation frequency $\omega = 1.4 \times 10^9$ Hz.^{18,19}

Similarly, in Fig. 6 are presented the pulse profiles for the “interpulse” of curvature radiation from PSR J1828-1101. Fig. 6a shows the plots of I (black), Q (red), U (green) and V (blue) created based on the actual data obtained from observations at 1.4 GHz. Corresponding to this, Fig. 6b shows our theoretical plots of \mathcal{I} (black), \mathcal{Q} (red), \mathcal{U} (green) and \mathcal{V} (blue) for the emission by a Gaussian particle bunch in curved (solid line) and flat (dashed line) spacetimes: they are modeled with the

¹⁷ The approximation is employed to compute our theoretical pulse profiles in Figs. 5 and 6. However, while we compute Gaussian modulations of $S'(\phi - \phi_*)$ explicitly, only the effects of Gaussian modulations of $\mathcal{O}((\theta - \theta_*))$ are treated numerically, with no explicit information about θ_o and σ_{θ} ; we use this effective method since the modulations of $\mathcal{O}((\theta - \theta_*))$ that depend on θ_o and σ_{θ} are not well constrained by the observational data.

¹⁸ In Figs. 5 and 6 our pulse profile curves are plotted with a vertical axis scale relative to the maximum of the intensity \mathcal{I} for the main pulse in curved spacetime, which is set to be 1.

¹⁹ The Gaussian modulations of $\mathcal{O}((\theta - \theta_*))$ from (90) have been treated numerically. Among others, the effect of the modulation for the Stokes U is notable; it has caused the pulse profile curve to shift upward [34], which has moved the zero of the curve to the left as a result.

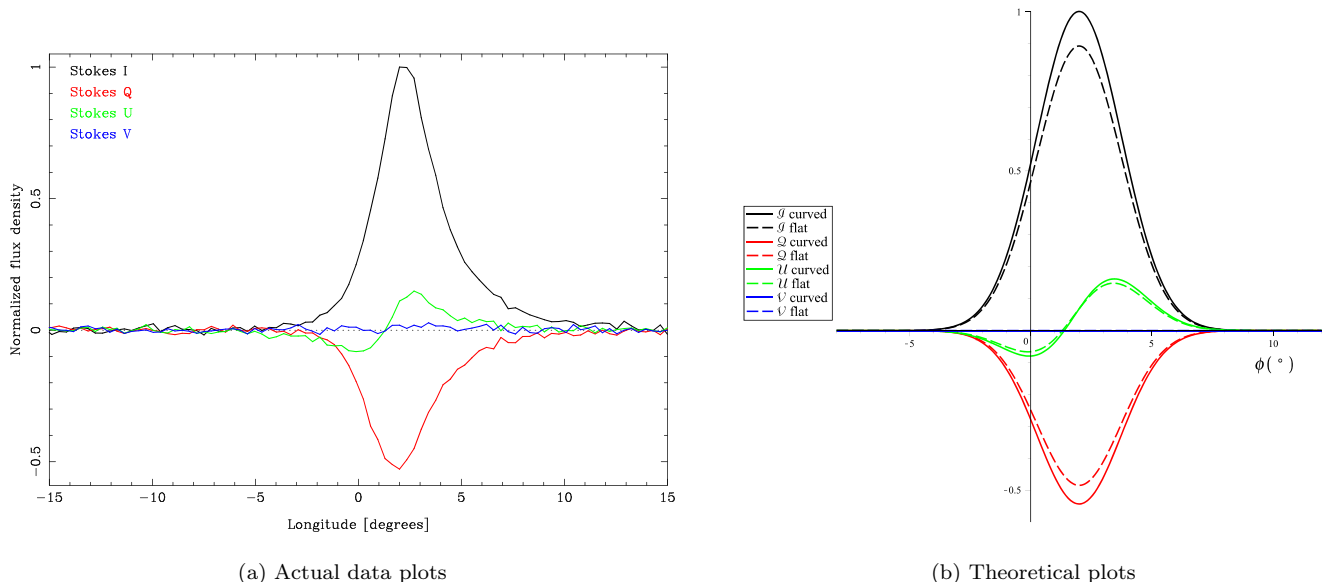


FIG. 5: Pulse profiles for the main pulse emission from PSR J1828-1101.

emission height $r_s \simeq 4.5 \times 10^6$ cm; the inclination angle $\alpha = 97^\circ.3$; the sight line impact angle $\varepsilon = -7^\circ.3$; the phase $\psi = 45^\circ$; the angular spread $\sigma_\phi = 0^\circ.03$; the peak location $\phi_o = 179^\circ.5$; the tuning factor $\tau = 10$; the scaling factor $\lambda = \frac{1}{60}$ (which matches the model pulse width to the observed width), for the same M , γ and ω .²⁰

Note that for Figs. 5b and 6b the values of r_s , α , ε and ω have been taken from Ref. [10], whereas the values of ψ , σ_ϕ , ϕ_o , τ , λ and γ have been chosen such that our theoretical plots match best with observational plots in Figs. 5a and 6a. Also, it should be noted that circular polarization as exhibited by V (blue) in Fig. 6a is entirely negative; hence, our \mathcal{V} (blue) in Fig. 6b has been modeled following this. Here our method can be described as follows. From Eq. (87), one can reexpress $V' = -V = E_L^* E_L - E_R^* E_R$ in the basis $\{\mathbf{e}_L, \mathbf{e}_R\}$, where $\mathbf{e}_L = \begin{bmatrix} 1 & i \\ 0 & 0 \end{bmatrix}^T$ and $\mathbf{e}_R = \begin{bmatrix} 1 & -i \\ 0 & 0 \end{bmatrix}^T$ denote left-hand and right-hand circular polarization, respectively [33]. However, in order to have the entirely negative support over the whole domain of ϕ , V' has to be reduced to $-pE_R^* E_R = -\frac{p}{2}I' + \frac{p}{2}V'$, where $0 < p \leq 1$; i.e., it has to be right-hand circularly polarized only.²¹ To have

²⁰ Similarly, the Gaussian modulations of $\mathcal{O}((\theta - \theta_*)$) from (90) have been treated numerically. Again, the effect of the modulation for the Stokes U is notable; it has caused the pulse profile curve to shift downward [34], which has moved the zero of the curve to the left as a result.

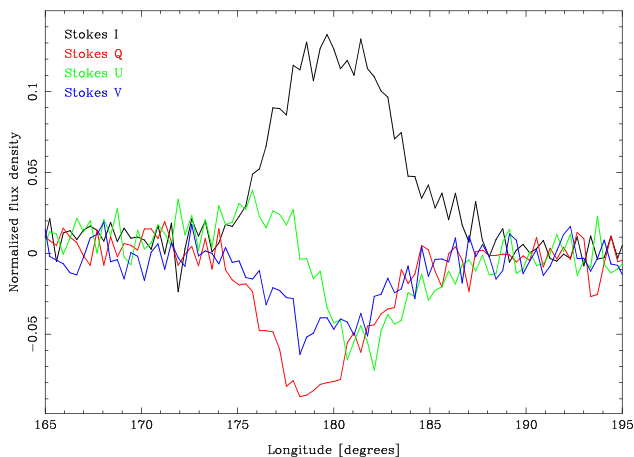
²¹ Suppose that V' is reduced to $v \equiv p_1 \tilde{E}_L^* \tilde{E}_L - p_2 \tilde{E}_R^* \tilde{E}_R$, where

the best match with V (blue) in Fig. 6a, we have chosen $p \approx 0.8$ and thus plotted our \mathcal{V} (blue) by modulating $-0.4I' + 0.4V'$ with the Gaussian function via Eq. (88).

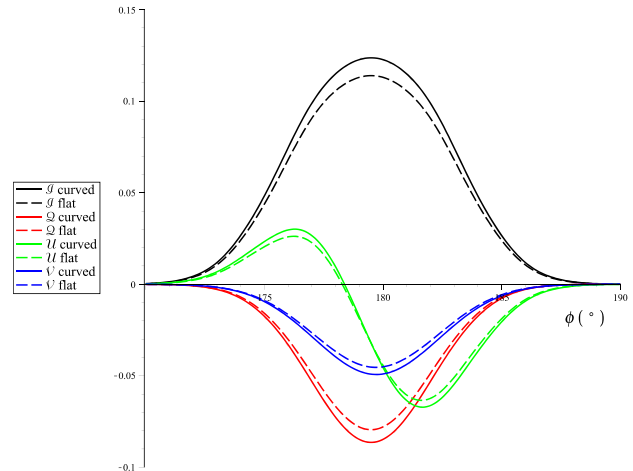
IV. SUMMARY AND CONCLUSIONS

We have investigated general relativistic effects in electromagnetism of a pulsar based on its magnetic dipole model defined in curved spacetime. Our analysis can be briefly summarized as follows. The magnetic field is described by a solution to Maxwell's equations in a spacetime geometry specially prescribed for an oblique rotator: a slowly rotating Schwarzschild geometry modified from the Kerr spacetime, with the frame-dragging frequency replaced by the pulsar rotation frequency (Sections IIB 1-IIB 3). The magnetic field in the curved

$0 \leq p_1, p_2 \leq 1$. Now, with $\tilde{E}_L = \frac{1}{\sqrt{2}}(\tilde{E}_\parallel + i\tilde{E}_\perp)$ and $\tilde{E}_R = \frac{1}{\sqrt{2}}(\tilde{E}_\parallel - i\tilde{E}_\perp)$, we can express $v = \frac{p_1 - p_2}{2}I' + \frac{p_1 + p_2}{2}V'$, due to Eqs. (84) and (87). However, if $v \leq 0$ everywhere in the domain of ϕ , the following must hold true always: $\frac{p_1 - p_2}{p_1 + p_2}(X^2 + Y^2) - 2\sin\psi XY \leq 0$, where $p_1 < p_2$, and $X = \mathcal{E}_o \omega \varphi (\delta^2 + \varphi^2) K_{1/3}(\frac{\omega}{3\omega_o}(\delta^2 + \varphi^2)^{3/2})$ and $Y = \mathcal{E}_o \omega (\delta^2 + \varphi^2) K_{2/3}(\frac{\omega}{3\omega_o}(\delta^2 + \varphi^2)^{3/2})$, defined via Eqs. (74), (77), (84) and (87). This inequality can be satisfied only if $p_1 = 0$ and $p_2 > 0$; i.e., $-\sin\psi(X + Y)^2 \leq (1 - \sin\psi)(X^2 + Y^2)$ for $0^\circ \leq \psi \leq 90^\circ$. Therefore, V' is eventually reduced to $v = -p_2 \tilde{E}_R^* \tilde{E}_R$, where $0 < p_2 \leq 1$.



(a) Actual data plots



(b) Theoretical plots

FIG. 6: Pulse profiles for the interpulse emission from PSR J1828-1101.

spacetime manifestly exhibits the effect of gravity: the stronger the closer to the surface of the neutron star. By means of the magnetic field in the curved spacetime, well-known issues such as very low-frequency magnetic dipole radiation for pulsar spin-down (Section III A) and pulse profiles of curvature radiation (Section III B 2) are extended to the context of general relativity. Also, these results are compared with their flat-spacetime counterparts so that the differences manifestly show the effects of gravity.

In this study, we have devoted considerable attention to the mechanism of pulsar radio emission in the context of general relativity: among other things, our primary focus has been on general relativistic effects on the pulse profiles of curvature emission. Well inside a pulsar magnetosphere, the magnetic field strength is very high, and so is the strength of gravity of the neutron star. The effect of gravity is so intense as to modify the magnetic field lines in this region: the curvature radii of the field lines would decrease due to strong gravity (Eqs. (62) and (63)). This would increase the frequency of curvature radiation emitted by charges moving along the magnetic field lines in the region (Eq. (66)), and in turn, modify the pulse profiles (Eqs. (74)-(77)). Figs. 5 and 6 show this clearly. Overall, the effect of gravity increases the magnitude of our pulse profile curves for intensity \mathcal{I} , linear polarization \mathcal{Q} and \mathcal{U} , and circular polarization \mathcal{V} modeled for Gaussian particle-bunch radiation: from Eqs. (66) and (74)-(77) magnitude $\sim \mathcal{E}_o^2 \sim \omega_o^2 \sim \rho^{-2}$, and therefore magnitude (curved) $>$ magnitude (flat).

We have taken the pulsar PSR J1828-1101 as an example, in which the pulse profiles of the main and interpulse emissions from the regions $3.5R_* \simeq 3.5 \times 10^6$ cm and $4.5R_* \simeq 4.5 \times 10^6$ cm, respectively, above the surface of the neutron star of mass $M \simeq 1.4 M_\odot$ ($m = GM/c^2 \simeq 2.065 \times 10^5$ cm) have shown that magnitude (flat) is about 89% and 92% of magnitude (curved) for the main pulse and the interpulse, respectively. This clearly exhibits the effect of gravity, which is due to the locations of emissions being relatively close to the surface of the star, where gravity is strong enough to affect electromagnetism of the pulsar.

Through our analysis based on general relativity, it is of great interest to see the gravitational effects in electromagnetism of a pulsar; especially, the effects on the pulse profiles. However, while actual observations of pulsars are indeed believed to contain these effects, it would be regarded as extremely difficult to disentangle and to identify them alone from observational data. Despite theoretical interest, the effects make a difference by 8% to 11% only, and therefore their testability is beyond the current detection capabilities since the absolute magnitude of the pulse profiles is not precisely predictable; not even the order of magnitude. We leave a discussion of this issue to a follow-up study.

ACKNOWLEDGMENTS

D.-H. Kim acknowledges financial support from the National Research Foundation of Korea (NRF) via Basic Research Grants NRF-2018R1D1A1B07051276 and NRF-2021R1I1A1A01054781. S. Trippe acknowledges financial support from the NRF via Basic Research Grant NRF-2019R1F1A1059721. We are grateful to Dr. Simon Johnston for providing the data for J1828-1101. The Parkes telescope is part of the Australia Telescope National Facility which is funded by the Commonwealth of Australia for operation as a National Facility managed by CSIRO.

Appendix A: Transformation between the Inertial Frame and the Corotating Frame

In the Cartesian representation, we have the relation between the two frames, $\mathbf{x} \equiv (x, y, z)$ (inertial frame) and $\mathbf{x}' \equiv (x', y', z')$ (obliquely corotating frame):

$$x' = -\sin(\Omega t)x + \cos(\Omega t)y, \quad (\text{A1})$$

$$y' = -\cos\alpha \cos(\Omega t)x - \cos\alpha \sin(\Omega t)y + \sin\alpha z, \quad (\text{A2})$$

$$z' = \sin\alpha \cos(\Omega t)x + \sin\alpha \sin(\Omega t)y + \cos\alpha z. \quad (\text{A3})$$

Fig. 2 illustrates how these two frames are related to each other.

By means of Eq. (A3) and

$$\cos\theta' = \frac{z'}{r} \quad (\text{A4})$$

together with

$$x = r \sin\theta \cos\phi, \quad (\text{A5})$$

$$y = r \sin\theta \sin\phi, \quad (\text{A6})$$

$$z = r \cos\theta, \quad (\text{A7})$$

one can establish

$$\cos\theta' = \cos\alpha \cos\theta + \sin\alpha \sin\theta \cos(\phi - \Omega t). \quad (\text{A8})$$

This is known as the spherical law of cosines, which can alternatively be obtained from consideration of a spherical triangle on the surface of the 2-sphere. In Section IIB, it gives a definition of the ‘‘magnetic colatitude’’.

Equivalent to Eqs. (A1)-(A3) are the relations between the basis vectors:

$$\begin{bmatrix} \mathbf{e}_{x'} \\ \mathbf{e}_{y'} \\ \mathbf{e}_{z'} \end{bmatrix} = \mathbf{T} \begin{bmatrix} \mathbf{e}_x \\ \mathbf{e}_y \\ \mathbf{e}_z \end{bmatrix}, \quad (\text{A9})$$

where

$$\mathbf{T} \equiv \begin{bmatrix} -\sin(\Omega t) & \cos(\Omega t) & 0 \\ -\cos\alpha \cos(\Omega t) & -\cos\alpha \sin(\Omega t) & \sin\alpha \\ \sin\alpha \cos(\Omega t) & \sin\alpha \sin(\Omega t) & \cos\alpha \end{bmatrix}. \quad (\text{A10})$$

A set of basis vectors in spherical polar coordinates $(\mathbf{e}_{\hat{r}}, \mathbf{e}_{\hat{\theta}}, \mathbf{e}_{\hat{\phi}})$ can be obtained by rotating the Cartesian set $(\mathbf{e}_x, \mathbf{e}_y, \mathbf{e}_z)$:

$$\begin{bmatrix} \mathbf{e}_{\hat{r}} \\ \mathbf{e}_{\hat{\theta}} \\ \mathbf{e}_{\hat{\phi}} \end{bmatrix} = \mathbf{R} \begin{bmatrix} \mathbf{e}_x \\ \mathbf{e}_y \\ \mathbf{e}_z \end{bmatrix}, \quad (\text{A11})$$

where

$$\mathbf{R} = \begin{bmatrix} \sin\theta \cos\phi & \sin\theta \sin\phi & \cos\theta \\ \cos\theta \cos\phi & \cos\theta \sin\phi & -\sin\theta \\ -\sin\phi & \cos\phi & 0 \end{bmatrix}. \quad (\text{A12})$$

The same argument holds true between $(\mathbf{e}_{\hat{r}}, \mathbf{e}_{\hat{\theta}'}, \mathbf{e}_{\hat{\phi}'})$ and $(\mathbf{e}_{x'}, \mathbf{e}_{y'}, \mathbf{e}_{z'})$, with (θ, ϕ) replaced by (θ', ϕ') :

$$\begin{bmatrix} \mathbf{e}_{\hat{r}} \\ \mathbf{e}_{\hat{\theta}' } \\ \mathbf{e}_{\hat{\phi}' } \end{bmatrix} = \mathbf{R}' \begin{bmatrix} \mathbf{e}_{x'} \\ \mathbf{e}_{y'} \\ \mathbf{e}_{z'} \end{bmatrix}, \quad (\text{A13})$$

where

$$\mathbf{R}' = \begin{bmatrix} \sin\theta' \cos\phi' & \sin\theta' \sin\phi' & \cos\theta' \\ \cos\theta' \cos\phi' & \cos\theta' \sin\phi' & -\sin\theta' \\ -\sin\phi' & \cos\phi' & 0 \end{bmatrix}. \quad (\text{A14})$$

Combining the transformations given by Eqs. (A10), (A12) and (A14), and after somewhat complicated algebraic manipulation, the transformation between the coordinate frames (r, θ, ϕ) and (r, θ', ϕ') can be finally determined:

$$\begin{bmatrix} \mathbf{e}_{\hat{r}} \\ \mathbf{e}_{\hat{\theta}} \\ \mathbf{e}_{\hat{\phi}} \end{bmatrix} = \mathbf{M} \begin{bmatrix} \mathbf{e}_{\hat{r}} \\ \mathbf{e}_{\hat{\theta}' } \\ \mathbf{e}_{\hat{\phi}' } \end{bmatrix}, \quad (\text{A15})$$

where

$$\mathbf{M} = \mathbf{R}\mathbf{T}^{-1}\mathbf{R}'^{-1} = \begin{bmatrix} 1 & 0 & 0 \\ 0 & \frac{\cos \alpha \sin \theta - \sin \alpha \cos \theta \cos(\phi - \Omega t)}{\frac{\sin \theta'}{\sin \alpha \sin(\phi - \Omega t)}} & \frac{-\sin \alpha \sin(\phi - \Omega t)}{\frac{\sin \theta'}{\sin \alpha \sin(\phi - \Omega t)}} \\ 0 & \frac{\sin \alpha \sin(\phi - \Omega t)}{\sin \theta'} & \frac{\cos \alpha \sin \theta - \sin \alpha \cos \theta \cos(\phi - \Omega t)}{\sin \theta'} \end{bmatrix}, \quad (\text{A16})$$

and θ' is defined through Eq. (A8).

Appendix B: Description of Motion of a Charge in a Specially Chosen Cartesian Frame

In Section III B 1 the trajectory ξ_s , the velocity $\dot{\xi}_s$ and the acceleration $\ddot{\xi}_s$ of a source charge along a magnetic field line are reexpressed in a Cartesian frame specially chosen for computational convenience, as given by Eqs. (70)-(72). These Cartesian expressions can be obtained through multiple coordinate transformations of the initial spherical polar representations (54)-(56).

The spherical polar representations of ξ_s , $\dot{\xi}_s$ and $\ddot{\xi}_s$ in Eqs. (54)-(56) can be projected into a Cartesian frame via Eq. (A13) with $\phi' = 0$:

$$\xi_s = r_s (\sin \theta'_s, 0, \cos \theta'_s), \quad (\text{B1})$$

$$\begin{aligned} \dot{\xi}_s &= \beta c \\ &\times \left(\frac{[1 - g(r_s)] \sin \theta'_s}{\sqrt{g^2(r_s) + \tan^2 \theta'_s}}, 0, \frac{-[g(r_s) + \tan^2 \theta'_s] \cos \theta'_s}{\sqrt{g^2(r_s) + \tan^2 \theta'_s}} \right), \end{aligned} \quad (\text{B2})$$

$$\begin{aligned} \ddot{\xi}_s &= \frac{\beta^2 c^2}{\rho} \\ &\times \left(\frac{-[g(r_s) + \tan^2 \theta'_s] \cos \theta'_s}{\sqrt{g^2(r_s) + \tan^2 \theta'_s}}, 0, \frac{[1 - g(r_s)] \sin \theta'_s}{\sqrt{g^2(r_s) + \tan^2 \theta'_s}} \right). \end{aligned} \quad (\text{B3})$$

From this we find $\dot{\xi}_s \cdot \ddot{\xi}_s = 0$ but $\xi_s \cdot \dot{\xi}_s \neq 0$; that is, $\dot{\xi}_s$ and $\ddot{\xi}_s$ are perpendicular to each other, but ξ_s and $\dot{\xi}_s$ are not, which results in $-\xi_s$ and $\ddot{\xi}_s$ not being parallel to each other.

Now, in order to redefine ξ_s , $\dot{\xi}_s$ and $\ddot{\xi}_s$ in another Cartesian frame, one can transform

$$\xi_s^{\text{N}} = \xi_s - \overrightarrow{OO^{\text{N}}}, \quad (\text{B4})$$

where $O \equiv (0, 0, 0)$ is the fixed origin, and O^{N} is a new origin, which makes the centre for an instantaneous circle of radius ρ passing through the point ξ_s given by (B1) (see Fig. 4). Through some analysis, it can be shown that

$$\overrightarrow{OO^{\text{N}}} = (r_s \sin \theta'_s + \rho \cos \theta'_s, 0, r_s \cos \theta'_s - \rho \sin \theta'_s), \quad (\text{B5})$$

which is not fixed, but varies with t_{R} through $r_s(t_{\text{R}})$ and $\theta'_s(t_{\text{R}})$. Then by Eqs. (B1), (B4) and (B5) we have

$$\xi_s^{\text{N}} = (-\rho \cos \theta'_s, 0, \rho \sin \theta'_s). \quad (\text{B6})$$

With the substitution $\theta'_s = \vartheta + \pi/2$, we finally obtain

$$\xi_s^{\text{N}} = \rho (\sin \vartheta, 0, \cos \vartheta). \quad (\text{B7})$$

Differentiating both sides of Eq. (B7) with respect to t_{R} , we have

$$\dot{\xi}_s^{\text{N}} = \rho (\dot{\vartheta} \cos \vartheta, 0, -\dot{\vartheta} \sin \vartheta). \quad (\text{B8})$$

With $\theta'_s(t_{\text{R}}) = \vartheta(t_{\text{R}}) + \pi/2$, Eq. (66) leads to

$$\dot{\vartheta} = \frac{\beta c}{\rho}. \quad (\text{B9})$$

Then using this for Eq. (B8), we obtain

$$\dot{\xi}_s^{\text{N}} = \beta c (\cos \vartheta, 0, -\sin \vartheta). \quad (\text{B10})$$

Similarly, we further obtain

$$\ddot{\xi}_s^{\text{N}} = \beta c (-\dot{\vartheta} \sin \vartheta, 0, -\dot{\vartheta} \cos \vartheta) = -\frac{\beta^2 c^2}{\rho} (\sin \vartheta, 0, \cos \vartheta). \quad (\text{B11})$$

Dropping the superscript N from Eqs. (B7), (B10) and (B11), we have exactly reproduced the expressions (70)-(72). Note that in this representation $\xi_s \cdot \dot{\xi}_s = 0$ and $\dot{\xi}_s \cdot \ddot{\xi}_s = 0$; that is, $\xi_s \perp \dot{\xi}_s$, $\dot{\xi}_s \perp \ddot{\xi}_s$, and $-\xi_s \parallel \ddot{\xi}_s$. This results from redefining ξ_s , $\dot{\xi}_s$ and $\ddot{\xi}_s$ in the special Cartesian frame by moving the origin from O to O^{N} , following Eq. (B4).

Appendix C: Pulse Profiles Expressed in the Rotation Phase ϕ

In Section III B 1 $\hat{\mathbf{r}}$, the unit vector for the observational direction for a distant observer is given by Eq. (73), being parametrized by the azimuthal angle φ , as expressed in the special Cartesian frame introduced in Appendix B. This is in contrast to the motion of a source charge along a magnetic field line, which is parametrized by the polar angle ϑ . However, in consideration of the analyses in Appendices A and B, one can identify

$\theta' = \vartheta + \pi/2$ and φ with the magnetic colatitude and azimuth, respectively.

As shown in Section III B 2, the pulse profiles based on the Stokes parameters, written as functions of the magnetic azimuth φ as given by Eqs. (74)-(77), can be plotted against the rotation phase ϕ instead of φ . This requires the transformation between φ and ϕ , which is given through the analysis below.

In the corotating frame described in Appendix A, the magnetic azimuth can be identified as $\varphi = \pi/2 - \phi'$. Then by means of Eqs. (A1) and (A2) together with Eqs. (A5)-(A7), one can write down

$$\begin{aligned} \frac{x'}{r} &= \sin \theta' \cos \phi' = \sin \theta' \sin \varphi \\ &= \sin \theta \sin (\phi - \Omega t), \end{aligned} \quad (\text{C1})$$

$$\begin{aligned} \frac{y'}{r} &= \sin \theta' \sin \phi' = \sin \theta' \cos \varphi \\ &= \sin \alpha \cos \theta - \cos \alpha \sin \theta \cos (\phi - \Omega t). \end{aligned} \quad (\text{C2})$$

Combining these two, we obtain the conversion expres-

sion between φ and ϕ :

$$\varphi = \arctan \left(\frac{\sin \theta \sin (\phi - \Omega t)}{\sin \alpha \cos \theta - \cos \alpha \sin \theta \cos (\phi - \Omega t)} \right). \quad (\text{C3})$$

For radiation from a source charge at $\theta_s = \alpha + \varepsilon$ on a magnetic field line at $t = 0$, the expression reduces to

$$\varphi = \arctan \left(\frac{\sin (\alpha + \varepsilon) \sin \phi}{\sin \alpha \cos (\alpha + \varepsilon) - \cos \alpha \sin (\alpha + \varepsilon) \cos \phi} \right), \quad (\text{C4})$$

where α and ε denote the inclination angle and the sight line impact angle, respectively. It can be checked from (C3) that $\varphi \rightarrow -\phi$ in the alignment limit $\alpha \rightarrow 0$. Also, from (C4) it can be shown that for $\phi \ll 1$,

$$\varphi \simeq -\frac{\sin (\alpha + \varepsilon)}{\sin \varepsilon} \phi + \mathcal{O}(\phi^2). \quad (\text{C5})$$

The pulse profiles (74)-(77) are dependent upon the curvature radius ρ through ω_o given by Eq. (66). Along with the conversion expression (C4) above, the curvature radius as given by Eq. (63) should also be reexpressed. By means of Eq. (A8), with $\theta_s = \alpha + \varepsilon$, the magnetic colatitude θ'_s is reduced to

$$\cos \theta'_s = \cos \alpha \cos (\alpha + \varepsilon) + \sin \alpha \sin (\alpha + \varepsilon) \cos (\phi - \Omega t). \quad (\text{C6})$$

Plugging this into Eq. (63), the curvature radius can be finally written as

$$\rho = r_s \left[1 + \frac{g^2(r_s) [\cos \alpha \cos (\alpha + \varepsilon) + \sin \alpha \sin (\alpha + \varepsilon) \cos \phi]^2}{1 - [\cos \alpha \cos (\alpha + \varepsilon) + \sin \alpha \sin (\alpha + \varepsilon) \cos \phi]^2} \right]^{1/2}. \quad (\text{C7})$$

REFERENCES

- [1] D.R. Lorimer, Binary and millisecond pulsars. *Living Rev. Relat.* **11**, 8 (2008). arXiv:0811.0762 [astro-ph]
- [2] B. Cerutti, A.M. Beloborodov, Electrodynamics of pulsar magnetospheres. *Space Sci. Rev.* **207**, 111 (2017). arXiv:1611.04331 [astro-ph.HE]
- [3] Q. Yuan, B. Zhang, Millisecond pulsar interpretation of the Galactic center gamma-ray excess. *J. High Energy Astrophys.* **3**, 1 (2014). arXiv:1404.2318 [astro-ph.HE]
- [4] C. Eckner et al., Millisecond pulsar origin of the Galactic center excess and extended gamma-ray emission from Andromeda: a closer look. *Astrophys. J.* **862**, 79 (2018). arXiv:1711.05127 [astro-ph.HE]
- [5] F. Özel, P. Freire, Masses, radii, and equation of state of neutron stars. *Annu. Rev. Astron. Astrophys.* **54**, 401 (2016). arXiv:1603.02698 [astro-ph.HE]
- [6] R.T. Gangadhara, Pulsar radio emission altitude from curvature radiation. *Astrophys. J.* **609**, 335 (2004). arXiv:astro-ph/0312081
- [7] D. Mitra, X.H. Li, Comparing geometrical and delay radio emission heights in pulsars. *Astron. Astrophys.* **421**, 215 (2004). arXiv:astro-ph/0312560
- [8] R.N. Manchester, G.B. Hobbs, A. Teoh, M. Hobbs, The Australia telescope national facility pulsar catalogue. *Astron. J.* **129**, 1993 (2005). arXiv:astro-ph/0412641
- [9] J.M. Rankin et al., Toward an empirical theory of pulsar emission XII: exploring the physical conditions in mil-

- lisecond pulsar emission regions. *Astrophys. J.* **845**, 23 (2017). arXiv:1710.11465 [astro-ph.HE]
- [10] S. Johnston, M. Kramer, On the beam properties of radio pulsars with interpulse emission. *Mon. Not. R. Astron. Soc.* **490**(4), 4565 (2019). arXiv:1910.04550 [astro-ph.HE]
- [11] S. Sengupta, General relativistic effects on the induced electric field exterior to pulsars. *Astrophys. J.* **449**, 224 (1995)
- [12] K. Konno, Y. Kojima, General relativistic modification of a pulsar electromagnetic field. *Prog. Theor. Phys.* **104**, 1117 (2000)
- [13] L. Rezzolla, B.J. Ahmedov, J.C. Miller, General relativistic electromagnetic fields of a slowly rotating magnetized neutron star - I. Formulation of the equations. *Mon. Not. R. Astron. Soc.* **322**, 723 (2001). arXiv:astro-ph/0011316
- [14] M. Ruiz, V. Paschalidis, S.L. Shapiro, Pulsar spin-down luminosity: Simulations in general relativity. *Phys. Rev. D* **89**, 084045 (2014). arXiv:1402.5412 [astro-ph.HE]
- [15] J. Pétri, General-relativistic force-free pulsar magnetospheres. *Mon. Not. R. Astron. Soc.* **455**, 3779 (2016). arXiv:1511.01337 [astro-ph.HE]
- [16] J.A. Petterson, Magnetic field of a current loop around a Schwarzschild black hole. *Phys. Rev. D* **10**, 3166 (1974)
- [17] V.S. Beskin et al., *Accretion Disks, Jets and High-Energy Phenomena in Astrophysics: Les Houches Session LXXVIII, July 29 – August 23, 2002* (Springer-Verlag, Berlin, 2003)
- [18] D.R. Lorimer, M. Kramer, *Handbook of Pulsar Astronomy* (Cambridge University Press, Cambridge, 2005)
- [19] D.B. Melrose, R. Yuen, Obliquely rotating pulsars: screening of the inductive electric field. *Astrophys. J.* **745**, 169 (2012). arXiv:1107.0100 [astro-ph.SR]
- [20] V.L. Ginzburg, L.M. Ozernoy, On gravitational collapse of magnetic stars. *Zh. Eksp. Teor. Fiz.* **47**, 1030 (1964)
- [21] J.L. Anderson, J.M. Cohen, Gravitational collapse of magnetic neutron Stars. *Astrophys. Space Sci.* **9**, 146 (1970)
- [22] R.H. Price, Nonspherical perturbations of relativistic gravitational collapse. II. Integer-spin, zero-rest-mass fields. *Phys. Rev. D* **5**, 2439 (1972)
- [23] R. Ruffini, M. Sasaki, On a semirelativistic treatment of the gravitational radiation from a mass thrust into a black hole. *Prog. Theor. Phys.* **66**, 1627 (1981)
- [24] B.W. Carroll, D.A. Ostlie, *An Introduction to Modern Astrophysics*, 2nd edn. (Pearson Addison-Wesley, San Francisco, 2007)
- [25] F.F. Kou, H. Tong, Rotational evolution of the Crab pulsar in the wind braking model. *Mon. Not. R. Astron. Soc.* **450**, 1990 (2015). arXiv:1501.01534 [astro-ph.HE]
- [26] M. Dovčiak, V. Karas, A. Lanza, Magnetic fields around black holes. *Eur. J. Phys.* **21**, 303 (2000). arXiv:astro-ph/0005216
- [27] M.A. Ruderman, P.G. Sutherland, Theory of pulsars: polar gaps, sparks, and coherent microwave radiation. *Astrophys. J.* **196**, 51 (1975)
- [28] A.G. Pacholczyk, *Radio Astrophysics: Nonthermal Processes in Galactic and Extragalactic Sources* (Freeman, San Francisco, 1970)
- [29] J.D. Jackson, *Classical Electrodynamics*, 2nd edn. (Wiley, London, 1976)
- [30] J.A. Gil, J.K. Snakowski, Curvature radiation and the core emission of pulsars. *Astron. Astrophys.* **234**, 237 (1990)
- [31] G.B. Rybicki, A.P. Lightman, *Radiative Processes in Astrophysics* (Wiley, New York, 1979)
- [32] R.T. Gangadhara, Circular polarization in pulsars due to curvature radiation. *Astrophys. J.* **710**, 29 (2010). arXiv:1001.2671 [astro-ph.HE]
- [33] S. Trippe, Polarization and polarimetry: a review. *J. Korean Astron. Soc.* **47**, 15 (2014). arXiv:1401.1911 [astro-ph.IM]
- [34] D. Kumar, R.T. Gangadhara, Relativistic model on pulsar radio emission and polarization. *Astrophys. J.* **746**, 157 (2012). arXiv:1201.0748 [astro-ph.HE]